

Simulating the transport and dispersal of volcanic ash clouds with initial conditions created by a 3D plume model

Zhixuan Cao^{1,2} Marcus Bursik³ Qingyuan Yang^{4,5} Abani Patra^{*,1,6}

¹ Mechanical and Aerospace Engineering Department, SUNY Buffalo, Buffalo, NY, USA

² Fluids Business Unit, ANSYS Inc, Lebanon, NH, USA

³ Center for Geohazards Studies, SUNY Buffalo, Buffalo, NY, USA

⁴ Earth Observatory of Singapore, Singapore, Singapore

⁵ The Asian School of the Environment, Nanyang Technological University, Singapore, Singapore

⁶ Data Intensive Studies Center, Tufts University, Medford, MA, USA

Correspondence*:

Abani Patra

abani.patra@tufts.edu

2 ABSTRACT

Volcanic ash transport and dispersion (VATD) models simulate atmospheric transport of ash from a volcanic source represented by parametrized concentration of ash with height. Most VATD models use a source of some prescribed shape calibrated against an empirical expression for the height-mass eruption rate (MER) relation. The actual vertical ash distribution in volcanic plumes usually varies from case to case and has complex dependencies on eruption source parameters and atmospheric conditions. We present here for the first time the use of a three-dimensional (3D) plume model to represent the ash cloud source without any assumption regarding plume geometry. By eliminating assumed behavior associated with a parametrized plume geometry, the predictive skill of VATD simulations is greatly improved. To date, no VATD simulation adopts initial conditions created from first principles based on a 3D plume simulation. We use our recently developed volcanic plume model based on a 3D smoothed-particle hydrodynamic Lagrangian method, and couple the output to a standard Lagrangian VATD model. We apply the coupled model to the Pinatubo eruption in 1991 to illustrate the effectiveness of the approach. Our investigation reveals that initial particle distribution in the vertical direction, including within the umbrella cloud, has more impact on transport of ash clouds than does the horizontal distribution. Comparison with satellite data indicates that ash particles are concentrated through the depth of the volcanic umbrella cloud, and much lower than the observed maximum plume height.

20 Keywords: VATD, volcano, 3D plume model, initial conditions, numerical simulation, SPH, Pinatubo, ash transport, ash dispersal

1 INTRODUCTION

Volcanic ash, the fine-grained fraction of tephra, can be widely dispersed to synoptic and global scales, and can lead to a degradation of air quality and pose threats to aviation (Tupper et al., 2007). Identification, tracking and modeling the future movement of volcanic ash help route and schedule flights to avoid ash

24 clouds. Numerical estimation of ash distribution using known and forecast wind fields is necessary if
25 we are to accurately predict ash cloud propagation and spread. Numerous volcanic ash transport and
26 dispersion (VATD) models have been developed by both civil and military aviation, and meteorological
27 agencies, to provide forecasts of ash cloud motion (Witham et al., 2007), such as Puff (Tanaka, 1991;
28 Searcy et al., 1998), NAME (Jones et al., 2007), HYSPLIT (Stein et al., 2015; Rolph et al., 2017) and
29 Ash3d (Schwaiger et al., 2012). New techniques have been integrated into VATDs to satisfy increasing
30 demands for different types of output, model accuracy and forecast reliability. This contribution explores a
31 forward modeling method for creating initial conditions for VATD simulations, which promises to reduce
32 the need for inversion or user intervention and improve forecasting.

33 Fero et al. (2009) and Stohl et al. (2011) showed that initial source conditions have significant effects on
34 simulation of volcanic ash transport. Constantinescu et al. (2021) proved that an enhanced initial condition
35 provides an overall better fit of the tephra deposit generated from an ash cloud than do models without
36 a disk-like source, demonstrating the significant impact of initial condition on ash dispersion. Besides
37 location of the eruption vent and timing of the release, traditional VATD simulation requires key global
38 descriptors of the volcanic plume, especially plume height, grain size, eruption duration and mass loading,
39 or alternatively, a mass eruption rate (MER). No matter how these global descriptors are obtained, they
40 are used to furnish the initial conditions for VATDs in the form of a line-source term of a spatio-temporal
41 distribution of particle mass. It is a common practice to pick values for these global descriptors using an
42 empirical expression for the height-MER relation. The values for the descriptors can also be found by
43 parameter calibration or inversion (e.g. Fero et al., 2008, 2009; Stohl et al., 2011; Zidikheri et al., 2017).
44 One-dimensional (1D) plume models serve as an alternative option to provide these values. For example,
45 Bursik et al. (2012) used the 1D model puffin (Bursik, 2001) to generate estimates of mass eruption
46 rate and grain size. In some cases, an extra step is adopted to spread ash particles from the line source
47 horizontally, resulting in an initial ash cloud in 3D space. The horizontal spreading depends on an empirical
48 expression as well. For example, the VATD model Puff spreads particles from the line source uniformly
49 in the horizontal direction within a given radius. Considering the complexities of volcanic eruptions, the
50 actual ash distribution in the initial cloud should vary from case to case and with time, making it difficult to
51 find one general expression that is suitable for all cases. It is useful therefore to investigate alternative ways
52 for creating initial ash clouds without assumptions regarding plume geometry, or numerical inversion. This
53 provides the major motivation of this paper.

54 VATD models can be categorized into Lagrangian particle tracking and Eulerian advection-diffusion types.
55 Among several available particle tracking models, such as, Hypact (Walko et al., 1995), Puff (Searcy et al.,
56 1998), CANERM (D'Amours, 1998), and HYSPLIT (Draxler and Hess, 1998) and advection-diffusion
57 models, such as Fall3D (Folch et al., 2009), and Ash3D (Schwaiger et al., 2012), we adopt a particle
58 tracking model, Puff, as the primary VATD model. Puff can accept a 3D point cloud description of the
59 starting ash cloud as an initial condition, which makes it technically easier to couple with a 3D Lagrangian
60 plume model. Puff initializes a discrete number of tracers that represent a sample of the eruption cloud, and
61 calculates transport, turbulent dispersion, and fallout for each representative tracer. A cylinder extending
62 vertically from the volcano summit to a specified plume height is the standard approach to provide a simple
63 model of the geometry of a typical ash column. Puff minimally requires horizontal wind field data. The
64 “restart” feature of Puff makes it feasible to accommodate the hand-off between a plume simulation and the
65 Puff simulation in terms of time and length scales. We use the Hybrid Single-Particle Lagrangian Integrated
66 Trajectory model (HYSPLIT) (Stein et al., 2015; Rolph et al., 2017) to better understand simulation results
67 from Puff in this study.

68 Besides parameter calibration, 1D plume models have been used to obtain global descriptors of volcanic
69 plumes. 1D plume models (e.g. Woods, 1988; Bursik, 2001; Mastin, 2007; de'Michieli Vitturi et al., 2015;
70 Folch et al., 2016; Pouget et al., 2016b) solve the equations of motion in 1D using simplifying assumptions,
71 and hence depend on estimation of certain parameters, especially those related to the entrainment of air,
72 which is evaluated based on two coefficients: a coefficient due to turbulence in the rising buoyant jet, and
73 one due to the crosswind field. Different 1D models adopt different entrainment coefficients based on a
74 specific formulation or calibration against well-documented case studies. The feedback from plume to
75 atmosphere is usually ignored in 1D models. While these 1D models generate well-matched results with
76 3D models for plumes that are dominated by wind (often called weak plumes) much greater variability
77 is observed for strong plume scenarios (Bursik et al., 2009; Costa et al., 2016). On the other hand, 3D
78 numerical models for volcanic plumes based on first principles and having few parametrized coefficients
79 (Oberhuber et al., 1998; Neri et al., 2003; Suzuki et al., 2005; Cerminara et al., 2016a; Cao et al., 2018)
80 naturally create a 3D ash cloud, which could serve directly as an initial state of the volcanic material for
81 VATDs. However, there is no VATD simulation using such 3D ash clouds as initial conditions. In this paper,
82 we will carry out VATD simulations using an initial state for the ash cloud based on 3D plume simulations,
83 generated with Plume-SPH (Cao et al., 2018, 2017). The implementation techniques described in this paper
84 can be applied to any combination of VATD model and 3D plume model even though our investigation is
85 based on a specific VATD model and plume model.

86 The 1991 eruption of Pinatubo volcano is used as a case study. Pinatubo erupted between June 12 and 16,
87 1991, after weeks of precursory activity. The climactic phase started on June 15 at 0441 UTC and ended
88 around 1341 UTC (Holasek et al., 1996a). The climactic phase generated voluminous pyroclastic flows,
89 and sent Plinian and co-ignimbrite ash and gas columns to great altitudes (Scott et al., 1996). The evolution
90 of the Pinatubo ash and SO₂louds was tracked using visible (Holasek et al., 1996a), ultraviolet (Total
91 Ozone Mapping Spectrometer; TOMS) (Guo et al., 2004a) and infrared sensors, including the Advanced
92 Very High-Resolution Radiometer (AVHRR) (Guo et al., 2004b). There is sufficient observational data to
93 estimate the eruption conditions for the climactic phase of the eruption (Suzuki and Koyaguchi, 2009). The
94 availability of calibrated eruption conditions and extensive observational data regarding ash cloud transport
95 make the Pinatubo eruption an ideal case study.

2 MATERIALS AND METHODS

96 2.1 Plume-SPH Model

97 Plume-SPH (Cao et al., 2018) is designed to describe an injection of well mixed solid and volcanic gas
98 from a circular vent above a flat surface into a stratified stationary atmosphere. The basic assumptions of
99 the model are:

- 100 1. Molecular viscosity and heat conduction is neglected since turbulent energy and momentum exchange
101 are dominant.
- 102 2. Erupted material consisting of solid with different size and mixture of gases is assumed to be well
103 mixed and behave like a single phase fluid (phase 2) which is valid for eruptions with fine particles and
104 ash.
- 105 3. Air, which is assumed to be a well mixed mixture of different gases, is assumed to be another phase
106 (phase 1).
- 107 4. Assume thermodynamic equilibrium and dynamic equilibrium between the two phases. As a result,
108 both phases share the common energy equation and momentum equations.

- 109 5. All other microphysical processes (such as the phase changes of H₂O aggregation, disaggregation,
 110 absorption of gas on the surface of solids, solution of gas into a liquid) and chemical processes are not
 111 considered in this model.
 112 6. The effect of wind is also not yet considered in this model.

Based on above assumptions, the governing equations of our model are given as:

$$\frac{\partial \rho}{\partial t} + \nabla \cdot (\rho \mathbf{v}) = 0 \quad (1)$$

$$\frac{\partial \rho \xi}{\partial t} + \nabla \cdot (\rho \xi \mathbf{v}) = 0 \quad (2)$$

$$\frac{\partial \rho \mathbf{v}}{\partial t} + \nabla \cdot (\rho \mathbf{v} \mathbf{v} + p \mathbf{I}) = \rho \mathbf{g} \quad (3)$$

$$\frac{\partial \rho E}{\partial t} + \nabla \cdot [(\rho E + p) \mathbf{v}] = \rho \mathbf{g} \cdot \mathbf{v} \quad (4)$$

- 113 where ρ is the density, \mathbf{v} is the velocity, ξ is the mass fraction of ejected material, \mathbf{g} is the gravitational
 114 acceleration, \mathbf{I} is a unit tensor. $E = e + K$ is the total energy which is a summation of kinetic energy K
 115 and internal energy e . An additional equation is required to close the system. In this model, the equation
 116 for closing the system is the following equation of state (EOS).

$$p = (\gamma_m - 1) \rho e \quad (5)$$

- 117 where

$$\gamma_m = R_m / C_{vm} + 1 \quad (6)$$

$$R_m = \xi_g R_g + \xi_a R_a \quad (7)$$

$$C_{vm} = \xi_s C_{vs} + \xi_g C_{vg} + \xi_a C_{va} \quad (8)$$

$$\xi_a = 1 - \xi \quad (9)$$

$$\xi_g = \xi \cdot \xi_{g0} \quad (10)$$

$$\xi_s = \xi - \xi_g \quad (11)$$

- 123 where, C_v is the specific heat with constant volume, R is the gas constant. ξ is the mass fraction of erupted
 124 material. The subscript m represents mixture of ejected material and air, s represents solid portion in the
 125 ejected material, g represents gas portion in the ejected material, a represents air, 0 represents physical
 126 properties of erupted material. ξ_{g0} is the mass fraction of vapor in the erupted material.

- 127 Three different boundary conditions are applied in this model. At the vent, temperature of erupted
 128 material T , eruption velocity \mathbf{v} , the mass fraction of vapor in erupted material ξ_{g0} and mass discharge
 129 rate \dot{M} are given. The pressure of erupted material p is assumed to be the same as ambient pressure for
 130 pressure-balanced eruption. The radius of the vent is determined from ρ , \dot{M} and \mathbf{v} . Non-slip wall boundary
 131 condition is applied to the flat ground, where we enforce the velocity to be zero. With further assumption
 132 that the ground is adiabatic, internal energy flux, which consists of heat flux and energy flux carried by
 133 mass flux, vanishes on the wall boundary. Pressure outlet boundary condition is applied to the surrounding
 134 atmosphere where the pressure is given. Except for the pressure, boundary values for density, velocity, and

135 energy are determined by numerical calculation naturally. The initial condition for Plume-SPH is created
 136 based on the atmosphere profile before the eruption.

137 The governing equations, EOS, boundary conditions, and initial conditions establish a complete mathematical
 138 model. The model is then discretized using smoothed particle hydrodynamics (SPH) method (Gingold
 139 and Monaghan, 1977). The computational domain is discretized by SPH particles. The current version,
 140 Plume-SPH (Cao et al., 2018) uses two types of SPH particles: 1) particles of phase 1 to represent ambient
 141 air, and 2) particles of phase 2 to represent erupted material. So before the eruption, the computational
 142 domain is fully occupied by particles of phase 1. During the eruption, particles of phase 2 are injected
 143 into the computational domain. The discretized model is then converted into computational software
 144 (Plume-SPH) based on a parallel data management framework (Cao et al., 2017).

145 The input parameters for Plume-SPH include the eruption condition at vent, the material properties, and
 146 atmosphere profile. The eruption parameters, material properties and atmosphere for the “Strong plume–no
 147 wind” case in the recent comparison study on eruptive column models (Costa et al., 2016) are adopted.
 148 Eruption conditions and material properties are listed in Table 1. Note that the density of erupted material
 149 at the vent and radius of the vent can be computed from the given parameters. The eruption pressure
 150 is assumed to be the same as the atmospheric pressure at the vent, hence is not given in the table. The
 151 vertical profiles of atmospheric properties were based on the reanalysis data from European Centre for
 152 Medium-Range Weather Forecasts (ECMWF) for the period corresponding to the climactic phase of the
 153 Pinatubo eruption.

154 Running of Plume-SPH updates physical quantities, such as temperature, velocity, and the position of
 155 SPH particles in each time step. During Plume-SPH simulation, SPH particles of phase 2, which represent
 156 the erupted material, are injected from the eruption vent into the computation domain with an initial
 157 injection velocity. As they move upwards, these particles will get mixed with SPH particles of phase 1,
 158 which represent the air, during the whole simulation. Their physics quantities get updated as well. After
 159 the simulation, the computation domain will be filled with SPH particles of both phase 1 and phase 2.
 160 Removing all SPH particles of phase 1 from the computation domain, all of the left SPH particles are these
 161 particles that represent the erupted material, which naturally forms a plume (see Fig. 1).

162 2.2 Puff and Initial Ash Cloud

163 Puff (Tanaka, 1991; Searcy et al., 1998) is a dynamic pollutant tracer model. The model is based on a 3D
 164 Lagrangian form of the fluid mechanics, in which the material transport is represented by the fluid motion,
 165 and diffusion is parameterized by a stochastic process of random walk. Here, the model is constructed by a
 166 sufficiently large number of Lagrangian tracer particles with a random variables $\mathbf{R}_i(t) = (x(t), y(t), z(t))$,
 167 where $i = 1 \sim M$, which represent position vectors of particles from the origin of the ash source at the
 168 time t . M is the total number of Lagrangian tracer particles, a sample of all the ash particles.

$$\mathbf{R}_i(t + \Delta t) = \mathbf{R}_i(t) + \mathbf{W}(t)\Delta t + \mathbf{Z}(t)\Delta t + \mathbf{S}_i(t)\Delta t \quad (12)$$

169 Here, \mathbf{W} accounts for local wind advection, \mathbf{Z} is generated by Gaussian random numbers and accounts
 170 for turbulent dispersion, and \mathbf{S} is the terminal gravitational fallout velocity or settling speed, which depends
 171 on a tracer’s size.

172 A collection of tracer particles can be used to start a Puff simulation. The tracer particles have three basic
 173 properties, age, size and position. The age of each particle is the elapsed time from when it was released.
 174 Ash particles in the initial ash cloud have zero age. Initial ash size distribution is assumed to be log-normal.

175 According to a mean and standard deviation provided by the user, Puff assigns size to each particle. Puff
 176 initializes the position of each particle according to semiempirical expressions. The height of each particle
 177 is determined according to the specified distribution from the surface (1000 mbar \cong 0 m) to the top of the
 178 plume height, H_{max} , which is given by the user. Puff also supports reading predefined initial ash clouds
 179 from a file, containing the coordinates of all tracer particles.

180 The commonly used vertical particle distribution in Puff is the Poisson distribution. For the Poisson
 181 distribution, the vertical height of ash particles is given by Eq. (13):

$$H = H_{max} - 0.5H_{width}P + H_{width}R \quad (13)$$

182 where P is an integral value drawn from a Poisson distribution of unit mean, R is a uniformly distributed
 183 random number between 0 and 1, H_{max} is the maximum plume height, H_{width} represents an approximate
 184 vertical range over which the ash will be distributed. So for Poisson distribution, the user can specify two
 185 parameters, H_{max} and H_{width} . Another commonly used vertical ash distribution in VATD simulation is
 186 Suzuki. For the Suzuki plume shape (Suzuki et al., 1983), the ash mass vertical distribution is assumed to
 187 follow the Eq. (Eq. (14)):

$$Q(z) = Q_m \frac{k^2(1 - z/H_{max})\exp(k(z/H_{max} - 1))}{H_{max} [1 - (1 + k)\exp(-k)]} \quad (14)$$

188 Where Q_m is the total mass of erupted material, k is shape factor, which is an adjustable constant that
 189 controls ash distribution with height. A low value of k gives a roughly uniform distribution of mass with
 190 elevation, while high values of k concentrate mass near the plume top. So for Suzuki distribution, besides
 191 the plume height H_{max} , there is another user specified parameter, k .

192 Puff initializes the horizontal distribution of ash particles according to semiempirical expression as well.
 193 Puff uses a uniformly distributed random process to determine ash particle locations in a circle centered
 194 on the volcano site. The maximum radius (at plume top) at which a particle can be located is given as
 195 “horizontal spread”. The horizontal displacement from a vertical line above the volcano is a random value
 196 within a circle of which the radius equals the “horizontal spread” multiplied by the ratio of the particle
 197 height H to the maximum H_{max} , see Eq. 15. So the resulting shape of the particle distribution within the
 198 plume is an inverted cone in which particles are located directly over the volcano at the lowest level and
 199 extend out further horizontally with increasing plume height.

$$r(H) = r_{max}H/H_{max}R \quad (15)$$

200 where $r(H)$ is the radius of the horizontal circle, within which all particles at the height of H are located.
 201 r_{max} is the horizontal spread. H is the height, R is an uniformly distributed random number between 0 and
 202 1.

203 In summary, particle distributions in the initial ash cloud are controlled by several parameters, for
 204 example, H_{max} , H_{width} , and r_{max} if the user chooses to use semiempirical expressions, Eq. (13) and (15).
 205 Users can optimize or calibrate these parameters to adjust the initial condition for Puff so that the simulated
 206 results match better with observations. Besides the initial ash cloud, other input parameters for Puff are
 207 diffusivity in the vertical and horizontal directions, start and end time of the eruption, and eruption duration.
 208 When creating initial conditions from output of Plume-SPH, the total number of Lagrangian tracers is the
 209 count of all SPH particles of phase 2 in the plume. The same total number of Lagrangian tracers are used

when creating the initial ash cloud based on semiempirical expressions. All input parameters for Puff are listed in Table 2.

2.3 Creation of Initial Ash Cloud From Plume-SPH Output

In this study, we convert the output of Plume-SPH into initial ash cloud which serves as the initial condition for Puff. The method proposed consists in generating the initial ash cloud directly from Plume-SPH, foregoing assumptions and estimates, or inverse modeling, regarding ash injection height and timing. The steps to create an initial ash cloud based on the raw output of Plume-SPH are shown in Fig. 1. The initial ash cloud is created from SPH particles of phase 2, which represents the erupted material in the model. After reaching the maximum rise height and starting to spread horizontally, particles of phase 2 form an initial umbrella cloud (Fig. 2). The 3D plume simulation is considered complete once the umbrella cloud begins to form. Parcels that will be transported by the ambient wind are those above the “corner” region, where mean plume motion is horizontal rather than vertical. With such consideration, we introduce an elevation threshold, which is the lower elevation limit of the ash that will be transported by the VATD. All SPH particles with elevation lower than the threshold are excluded when creating the initial ash cloud. The inflection point from vertical raising to horizontal spreading happens around 15 km according to the averaged vertical velocity ((d) in Fig. 2) and horizontal velocity ((e) in Fig. 2)). Below this inflection point, particle trajectories are primarily vertical in the stalk-like eruption column. Above this level, particle trajectories are primarily horizontal, as they flow into the umbrella cloud gravity current. So we choose 15 km to be the elevation threshold in this study.

Considering that SPH particles are only discretization points, each is assigned a grain size according to a given total grain size distribution (TGSD) (Paladio-Melosantos et al., 1996), and a concentration according to the mass and volumetric eruption rate. The Plume-SPH discretization points are thus switched to Puff Lagrangian tracer particles having grain sizes and concentrations. The coordinates of these tracer particles, which are initially in the local Cartesian coordinate system of Plume-SPH, are converted into Puff’s global coordinate system, which is given in terms of (*longitude, latitude, height*). Puff takes the initial ash cloud, consisting of the collection of Lagrangian tracer particles with grain size and concentration, and propagates from time t to time $t + \Delta t$ via solution to an advection/diffusion equation (Eq. (12)).

To summarize, there are four steps to create an initial ash cloud from the raw output of Plume-SPH:

1. filter by SPH particle type to select SPH particles that represent erupted material (phase 2)
2. filter by a mean velocity threshold to select the upper part (above the “corner” region) dominated by horizontal transport
3. switch SPH discretization points to Lagrangian tracer particles, by assigning grain size to each particle
4. convert coordinates of the SPH Lagrangian tracers into the VATDs’ geographic coordinate system

The features of the volcanic plume and resulting initial ash cloud used in the case study are shown in Fig. 2. It is important to point out that since both Plume-SPH and Puff are based on the Lagrangian method, there is no extra step of conversion between an Eulerian grid and Lagrangian particles.

2.4 Puff Restart

The plume and ash transport models are run at different time scales and length scales. The spatial and temporal resolutions of the plume simulations are much finer than those of the ash transport model. It takes tens of minutes (600 s in this case) for the Pinatubo plume to reach a steady height. However the eruption persisted for a few hours (9 hours for the climactic phase of Pinatubo eruption), and it may be necessary to track ash transport for days following an eruption. At present, it is too computationally expensive to

run 3D plume simulations of several hours in real time. In order to handle the difference in time scale, we mimic a continuing eruption with intermittent pulses releasing ash particles. In particular, we restart Puff at an interval of 600 s, i.e., the physical time of the plume simulation to reach a steady height. At every Puff restart, we integrate the output of the last Puff simulation and Plume-SPH into a new ash cloud. This new ash cloud serves as a new initial condition with which to restart a Puff simulation. A sketch demonstrating the overall restart process is shown in Fig. (3). The total number of Lagrangian tracer particles used in Puff thus equals the summed number of particles in all releases. The total number of tracer particles is therefore no longer a user-selected parameter. Fero et al. (2008) proposed using more realistic time-dependent plume heights. We do not adopt that strategy here for simplicity, although the idea would be straightforward in execution, given time-dependent eruption conditions.

3 RESULTS

Transport of volcanic ash resulting from the Pinatubo eruption on June 15, 1991, is simulated using two different initial conditions. The first type of initial condition is created in a traditional way according to user specified parameters (H_{max} , H_{width} and r_{max}) and the semiempirical plume shape expressions (Eq. (13) and (15)). We use the observed plume height (40 km) as H_{max} and adopt two other parameters from previous study(Fero et al., 2008). The second type of initial condition is created by the new method proposed in this paper. To create initial conditions using the new method described in this paper, the plume rise is simulated first by Plume-SPH. Then the initial ash cloud is obtained by processing the raw output of Plume-SPH following steps described in Sec. 2.3. Except for initial conditions, the simulation parameters that control the VATD simulation are the same for both simulations. Simulated ash transport results are compared against observations.

The simulation results using different initial conditions are compared with TOMS SO₂ and AVHRR BTD (Brightness Temperature Difference) ash cloud map imagery (Fig. 4). The Puff simulation results are post-processed by the following steps to calculate the relative concentration.

1. The 3D computational domain is discretized into a collection of cells (latitude, longitude, elevation), each cell is of size 0.2 degree × 0.2 degree × 1 km
2. Find the cell that has the maximum number of particles (tracer particles); say the maximum number of particles is N_{max} .
3. Exclude all cells that have fewer than five particles.
4. Calculate the relative concentration of each cell by dividing the number of particles in the cell by N_{max} .

In the contour, we plot the relative concentration of the cell that has maximum number of particles at a given (*latitude, longitude*). In addition to the relative concentration, we also plot the contours of maximum height of the ash cloud (Fig. 5), which is obtained by the following post-processing steps.

1. The 3D computational domain is discretized into a collection of cells (latitude, longitude, elevation), each cell is of size 0.2 degree × 0.2 degree × 1 km
2. Exclude all cells that have fewer than five particles.
3. The maximum height is the cell center height of the top cell among all cells with the same (*latitude, longitude*).

We also calculated the Figure of Merit in Space (FMS) according to the definition: FMS = (area of intersection of Puff forecast footprint and satellite image extent)/(area of union).

The differences between simulated ash transport by the “Semiempirical initial cloud + Puff” and “Plume-SPH+ Puff” conditions are significant. We first check the maximum relative concentration in Fig. 4. At 23 and 31 hours after the beginning of the climactic phase, the simulated ash concentration based on the initial conditions created from Plume-SPH is visibly closer to observation than that based on the initial condition generated from semiempirical expressions, especially in terms of the location of the highest concentration region. This is confirmed by the FMS, which is 0.249 (23 hours) and 0.269 (31 hours) for Plume-SPH results, and 0.063 (23 hours) and 0.065 (31 hours) for semiempirical initial clouds. Around 55 hours after the beginning of the climactic phase, the disparity between observation and simulation becomes more obvious. Ash in the “Semiempirical initial cloud + Puff” simulation is located far west of the observed, with a FMS value equal to 0.058. The high concentration area of the “Plume-SPH + Puff” simulation, even though closer to observation, has also propagated further downwind than in the observation. The FMS goes down to 0.085.

It is useful to compare the maximum cloud height in Fig. 5 with the wind field indicated in HYSPLIT forward trajectory tracking (Fig. 6). The comparison reveals that the ash cloud is being transported in two separate, main layers (directions) independently. From Fig. 6, we can see that the wind between elevations of 10 km and 15 km blew from north-east to south-west, while winds of higher elevation blew from east to west. This vertical wind shear naturally separated the ash cloud into two layers. In the “Semiempirical initial cloud + Puff” results, the lower elevation layer is missing, which is the most important factor causing differences between these two simulation results (Fig. 4). Even for the upper layer, the maximum cloud height of the “Semiempirical initial cloud + Puff” simulation results is higher than that of the “Plume-SPH+ Puff” simulation. Such differences cannot be captured by metrics based on footprint, such as FMS. At 55 hours after the eruption, the observed high concentration ash, which is at a relatively low elevation (inferred from the wind direction at different elevations in Fig. 6 and the eruption location), is missing in the “Plume-SPH + Puff ” simulation results. This leads to the large decrease of FMS values from 0.269 to 0.085. One possibility is that these ash clouds are from eruptions after the climactic phase. In our current simulation, we use the eruption condition for the climactic phase generating plume height for the climactic phase, but satellites see ash and SO₂ from all eruption phases.

The only difference in initial conditions between these two simulations is the distribution of ash parcels. The main difference between simulation results from the “Plume-SPH + Puff” and the “Semiempirical initial cloud + Puff” runs can thus be directly attributed to the initial ash particle distribution, which we discuss further in the following section.

3.1 Effect of plume height (H_{max})

In this section, we discuss the vertical distribution of ash particles in the initial ash cloud. The majority of volcanic ash particles are usually injected at an elevation lower than the plume height. For instance, Holasek et al. (1996a,b) reported the maximum Pinatubo plume height as ~ 39 km while the cloud heights were estimated at $\sim 20 - 25$ km. Self et al. (1996) reported that the maximum plume height could have been > 35 km, but that cloud heights were $23 - \sim 28$ km after $\sim 15 - 16$ hours. The neutral buoyancy height of the Pinatubo aerosol cloud was estimated with different methods at: $\sim 17 - 26$ km (lidar) by DeFoor et al. (1992), $\sim 20 - 23$ km (balloon) by Deshler et al. (1992), $\sim 17 - 28$ km (lidar) by Jäger (1992), and $\sim 17 - 25$ km (lidar) by Avdyushin et al. (1993). Based on comparison between simulated clouds with early infrared satellite imagery, Fero et al. (2008) reported that the majority of ash was transported between 16 km and 18 km. These observations make good physical sense, as particles are concentrated near the intrusion height of the umbrella cloud, not near the plume top, because the plume top is due to momentum overshoot. However, the empirical expressions for the height-MER relation, which are commonly adopted

336 to create initial conditions for VATD simulations, tend to place the majority of ash particles closer to the
337 top if one uses observed plume height in the empirical expressions.

338 Here we investigate two commonly used plume shapes, the Poisson (see Eq. (13)) and Suzuki (see Eq.
339 (14)). Particle distributions (in terms of mass percentage or particle number percentage) in the vertical
340 direction in the initial ash cloud are shown in Fig. 7. In that figure, the vertical particle distribution based
341 on Plume-SPH output is compared with the vertical particle distribution based on semiempirical shape
342 expressions. Both Poisson and Suzuki distributions in Fig. 7 take $H_{max} = 40$ km, which is close to the
343 reported observed plume height. When adopting the Poisson distribution, ((c) in Fig. 7), the majority of the
344 particles are between 30 - ~ 40 km. Obviously, the Poisson function distributes the majority of ash at a
345 higher elevation than was observed (e.g. Fero et al., 2008). As for the Suzuki distribution, (d) in Fig. 7, the
346 majority of ash particles also occur in a range that is significantly higher than 25 km. Note that in the plot
347 (d), the Suzuki constant k is set to 4, which is commonly used for sub-plinian and plinian eruption columns
348 (Pfeiffer et al., 2005). As for initial ash clouds in Plume-SPH simulations, most ash particles are distributed
349 between ~ 17 - 28 km, which matches well with observations. The plume height is also consistent with
350 observation.

351 For the Poisson distributions, the ash particles cannot be lower without changing the plume height. To
352 distribute the majority of ash particles at a lower elevation, the plume height must be reduced to a value
353 smaller than the observed plume height. Adjusting parameters such as plume height in the empirical
354 expression is actually the traditional source term calibration method. A set of initial ash clouds using
355 different plume heights based on the Poisson distribution is shown in Fig. 8. The plume heights adopted in
356 plume shape expressions are not obtained from any plume model or observation of plume height, but by
357 *a posteriori* calibration to later-observed ash cloud transport heights. For Suzuki distribution, adjusting
358 the Suzuki constant can adjust the distribution of ash particles in vertical direction. As shown in Fig. 7,
359 when k is equal to 1 (see (e)), the majority of ash particles are at a lower elevation than observation. With
360 $k = 3$ and $k = 6$ (figure (g) and (h)), the majority of ash particles are at a higher elevation than observation.
361 When k is set to 2 (see (f)), we can see that the majority of ash particles are roughly distributed in the range
362 17 - 28 km. But the shape does not look like a typical plume, as particles are more uniformly distributed in
363 the vertical direction. In addition, the “best fit” Suzuki constant is different from the typical value, which
364 is 4 (Pfeiffer et al., 2005), for sub-plinian and plinian eruptions, meaning that we can not apply previous
365 experiences into the semiempirical expression for this eruption.

366 The ash clouds created by the Poisson distribution with different plume heights are used as initial
367 conditions in Puff simulations, whose results are shown in Fig. 11. Except for the plume height, all other
368 parameters for creating an initial ash cloud are the same as those in Table 2. Of course, the range over which
369 the majority of ash particles is located is lower when using lower plume heights. Figure 11 thus shows that
370 the plume height has a significant influence on the ash transport simulation. The maximum heights of the
371 simulated ash cloud are completely different when using different H_{max} values in the Poisson expression.
372 When the plume height is 10 km, the ash lags behind that observed and its FMS is 0.055, which is very
373 close to FMS when H_{max} is 40 km. For the cases that H_{max} is 20 km and 30 km, the FMS values are 0.121
374 and 0.142 respectively. Taking 20 km as the plume height better represents the lower elevation portion of
375 the ash cloud, while taking 30 km as the plume height better represents the higher elevation portion of the
376 ash cloud.

377 Simulation results based on a calibrated plume height of 30 km show a footprint similar to those of
378 “Plume-SPH + Puff”, although smaller in terms of area. However, the initial ash cloud created by a Poisson
379 distribution with a plume height around 35 km generates the best match with observation in terms of FMS

metric, with the FMS value reaching 0.227. That is to say, a plume height lower than the real plume height is required by the Poisson plume shape to distribute ash particles at elevations comparable to the “true” ash distribution. Even for the best matched results, the high concentration area does not match with observation well.

It is clear that the initial condition of vertical ash distribution has dominant effect on VATD simulation, so it is critical for the forecast capability of VATD simulations to explore more accurate and adaptive ways for establishing the initial ash distribution, especially methods that do not rely on *a posteriori* parameter calibration or inversion.

3.2 Effect of Vertical Spread (H_{width})

In the previous section, we explored the effects of adjusting the plume height to change the vertical ash distribution at the source. In this section, we investigate the importance of another parameter in the semiempirical Poisson expression (Eq. (13)). We vary the “vertical spread”, H_{width} , in the range $\sim 3 - 10$ km. A set of initial ash clouds with different vertical spreads are shown in Fig. 8. Except for vertical spread, all other parameters for creating an initial ash cloud are the same as those in Table 2. The vertical range within which the majority of ash particles are located becomes narrower when a smaller value for the vertical spread parameter is used. The ash clouds based on different vertical spread parameters are then used as initial conditions in Puff simulations.

The VATD results are shown in Fig. 11. Adjusting the vertical spread changes particle distribution in the vertical direction, and thus, not surprisingly, affects the VATD simulation results. None of the VATD simulations based on initial ash clouds with vertical spreads equal to 3 km or 5 km yield better results than do VATD simulations based on initial conditions created by Plume-SPH (see Fig. 11). But when we take 10 km as the vertical spread, we get a FMS that is very close to Plume-SPH, even though the shape of the ash cloud footprint and the maximum height of the ash cloud are completely different.

The calibration tests on vertical spread, carried out here, are certainly not exhaustive. One could do a more comprehensive calibration throughout the multi-dimensional parameter space (for Poisson distribution, the parameter space is two dimensional) and find better results. In addition, with a more complicated semiempirical plume shape expression, one could have more control over plume shape and might be able to get an initial condition that yields a more accurate ash transport forecast. However, more complicated and adaptable plume shape expressions imply a higher dimensional parameter space, which requires more effort in calibration, even though the degrees of freedom to adjust plume shape are still limited. Creating initial conditions based on 3D plume simulations avoids such parameter calibration.

3.3 Horizontal Ash Distribution

The differences between the semiempirical plume particle distribution and actual (or simulated by the 3D plume model) are not only in the vertical direction. The importance of the horizontal distance of each initial ash particle from a line extending upward from the volcano is investigated in this section. Puff uses a uniformly distributed random process to determine ash particle locations in a circle centered on the volcano site as described in section 2.2. For the output of Plume-SPH, an effective (maximum) radius is determined according to a given threshold of ash concentration, following Cerminara et al. (2016b). A time averaged, spatial integration of the dynamic 3D flow field is conducted to remove significant fluctuations in time and space. Fig. 9 compares the radius of the initial ash clouds created by 3D plume simulations with that assumed in the semiempirical plume shape expression adopted in Puff. It is impossible for the simple, assumed plume shapes to capture the complex and more realistic shapes developed by Plume-SPH. Additional parameterization may generate more reasonable shapes, but these would continue to be *ad*

423 *hoc*, none would likely have the potential fidelity of the 3D simulation to reality, and adding a temporally
424 changing distribution would be difficult.

425 Comparison between cross-sectional views of the initial ash clouds is shown in Fig. 10. The cross-
426 sectional view of horizontal particle distribution using the semiempirical method (last figure in Fig. 10)
427 is similar to a cross-sectional view of a simulated 3D plume, in a general sense. However, for simulated
428 3D plumes, the ash particle distribution in cross section varies with height, which factor would become
429 increasingly important with increasing wind speed, were wind speed to be included in the estimate of initial
430 plume shape. It is difficult for the semiempirical expressions to accommodate such a complex distribution.

431 Despite the obvious difficulty of correctly estimating ash distribution near the vent, or for short propagation
432 times, assigning different values for the horizontal spread has a negligible effect on VATD simulation
433 results at large time. We investigated horizontal spread values between 50 km and 1600 km to create initial
434 ash clouds; all of them generated similar results at large propagation times (> 1 day). Figure 11 shows
435 two different simulation results based on initial ash clouds with horizontal spread equal to 50 km and 600
436 km, respectively. No visible differences are apparent between them. The FMS values, 0.073 and 0.074,
437 respectively, are also very close. This implies that horizontal distribution has a less significant influence on
438 VATD simulation results than does vertical distribution for long distance or large time. Perhaps the most
439 important ramification of this result is that it means the time at which the “handshake” is made between
440 Plume-SPH and the VATD does not affect results significantly for relatively large distances and times.

4 DISCUSSION

4.1 Senthitivity of Other Inputs Parameters

441 Besides the initial ash cloud, other parameters for Puff simulations are: horizontal diffusivity, vertical
442 diffusivity, mean grain size, grain size standard deviation and total number of tracers. We present in this
443 subsection informal sensitivity studies on these parameters. We also investigate the influence of eruption
444 duration. The sensitivity analyses will serve as the basis for identifying possible sources of disparities
445 between simulation and observation.

446 Fero et al. (2008) simulated the volcanic ash transportation of Pinatubo eruption in 1991, he carried out
447 systematic sensitivity analysis with respect to input parameters of Puff and found that all other parameters
448 except for the plume height have negligible effect on long term ash transportation of Pinatubo. Inspired by
449 Fero et al. (2008), we carried out similar informal sensitivity analysis with much fewer sample points in
450 the parameter space and got similar results. Among the parameters explored, the eruption duration and
451 beginning time show the most obvious influence on simulated ash distribution, although the effect is still
452 small. To show the differences in an intuitive way, (a) - (c) in Fig. 12 shows simulated ash distribution
453 corresponding to 4.9 hours duration, 9 hours duration and 11 hours duration, respectively. After 72 hours,
454 relative to the simulation starting time, these three cases generate very similar results with tiny visible
455 differences. Daniele et al. (2009) did sensitivity analysis with respect to the input parameters of Puff on
456 different volcanoes and found that for eruptive eruptions, the most dominant factors are the wind field and
457 plume height, while all other input parameters are relatively less important. The significance of the wind
458 field has been confirmed by other researchers (Stefanescu et al., 2014, e.g) as well.

460 We conducted several simulations with eruption duration varying in the range of [5, 11] hours with
461 slightly different starting time of climactic phase. Table 3 lists all these simulations. However, only slight
462 visible differences are observed among the simulated ash transport outputs. We can see that the eruption
463 duration has negligible effects on long-term ash transport.

464 The new methodology for generating initial ash clouds introduces a new parameter: elevation threshold,
465 which was specified based on averaged vertical velocity and horizontal velocity. We carry out a separate,
466 informal sensitivity analysis on this parameter by varying the elevation threshold from 1.5 km (the height of
467 the vent) to 25 m. The simulated ash distributions show obvious differences, especially when the elevation
468 threshold is either very high or very low. However, varying the elevation threshold in the range of [12, 18]
469 km generates relatively small differences in ash transport simulation results. Figure 12 (d) and (e) compare
470 the simulated ash distributions corresponding to elevation thresholds of 1.5 km and 15 km. Compared with
471 the ash distribution for a threshold of 15 km, an extra long tail appears when using an elevation threshold
472 of 1.5 km. The maximum height of the tail is around 10 km. Adopting lower elevation thresholds adds
473 more tracer particles at lower elevation. As the winds at different elevations are different, the tracers at
474 lower elevations propagate in different directions. The HYSPLIT forward trajectory tracking indicates
475 that the wind between elevations of 10 km and 15 km blew from north-east to south-west, while winds of
476 higher elevation blew from east to west (see Fig. 6).

477 4.2 Other Sources of Disparities

478 The full range of research issues raised by numerical forecasting of volcanic clouds is diverse. We focused
479 on the effect of initial conditions in this paper. During the plume modeling, secondary factors, such as
480 microphysical processes, even though they play lesser roles, likely need to be included to improve accuracy
481 for a particular eruption. Wind fields are not considered in the current version of Plume-SPH, but for weak
482 plumes, wind plays such an important role that it has to be considered in the plume model. In addition,
483 eruption conditions are subject to change with time, even during the climactic phase of an eruption. For
484 example, ash just west of Pinatubo observed in satellite images does not show up in “Plume-SPH + Puff”
485 simulation results. This disparity is likely due to the fact that Pinatubo continued erupting (with smaller
486 plume height) after the climactic phase, while we only simulate the climactic phase. In the future, time-
487 dependent initial conditions for VATDs can be created from 3D plume simulations based on time-dependent
488 eruption conditions. Worth to mention that the eruption conditions at the vent are usually inferred from
489 observable information based on 1D plume models. Using a 3D plume model won’t reduce uncertainties
490 from the eruption conditions.

491 Assumption made in each VATD model is another source of errors. For example, a recent study by Osman
492 et al. (2020) demonstrated the great impact of GSD on modelled ash mass loadings using NAME(Jones
493 et al., 2007) to simulate historical eruptions of various VEIs. Other researchers (Beckett et al., 2015; Scollo
494 et al., 2008) have proven the significance of GSD using other VATD models. Their conclusion, however, is
495 different from our informal sensitivity study and other more comprehensive sensitivity studies using Puff.
496 This might be because of different assumptions made in different VATD models. These assumptions may
497 lead to underestimation or overestimation of certain factors, such as GSD. For example, at 55 hours after
498 eruption, we see an obvious FMS decrease of “Plume-SPH + Puff” results (see (f) in Fig. 5). One of the
499 important factors that contribute to the big decrease is the fact that these low elevation ash clouds (the west
500 south portion with small maximum heights) in simulation results are not observed by satellites. This is
501 probably because Puff underestimates the fallout of ash particles. That is to say, these low elevation ash
502 clouds should have already fallen onto the ground after 55 hours, but Puff failed to predict them to fall onto
503 ground. This explains why in the sensitivity studies using Puff, the GSD is always not impactful while
504 sensitivity analysis using other VATD models showing GSD is a significant factor.

505 One implicit assumption in the current method is that ash transportation is dominated by wind advection
506 (the passive dispersion approximation). However, during the growth of volcanic umbrella, the dominant
507 factors are various in different regimes (Pouget et al., 2016a) depending on characteristics of a particular

508 eruption. Webster et al. (2020) suggested that the lateral spread by the intrusive gravity current dominates
509 the transport of the ash cloud in this stage. A few studies by Larry Mastin (Mastin et al., 2014; Mastin
510 and Van Eaton, 2020) also showed that neglecting the umbrella cloud formation for larger eruptions led to
511 significantly different footprints for the resulting VATD fallout maps. Their studies imply that including
512 mapped velocities of the plume as a perturbation on the winds can better capture the radial spreading of
513 umbrella. In the current method, the 3D plume model generated initial ash cloud has a radius around 25
514 km. For the Pinatubo 1991 eruption, the passive dispersion approximation can be reasonably applied when
515 radius is greater than 450 km, and can be fully valid only when the radius is greater than 1800 km (Costa
516 et al., 2013). So the umbrella stage during the ash transportation is very likely oversimplified in current
517 simulation. It is computationally too expensive for the Plume-SPH model to continue simulation until the
518 plume radius reaches, at least, for example, 450 km. An additional umbrella model, with much coarse
519 resolution and simplified physics, in between the plume model and the VATD model would presumably
520 better model the whole ash transportation process.

521 Besides the errors from assumptions in the model, errors are also introduced from the reanalysis wind
522 field data and the satellite observations, which are retrievals, with their associated errors, rather than the
523 “truth.” In addition, metrics based on footprint can not account for the disparities at different height and ash
524 concentration. Comparing the simulation and observation purely based on footprint based metric sometimes
525 is biased.

526 4.3 Summary

527 This paper presents, for the first time, VATD simulations using initial source conditions created by a 3D
528 plume model. Traditional VATD simulations use initial conditions created according to a semiempirical
529 plume shape expression. A case study of the 1991 Pinatubo eruption demonstrates that a 3D plume model
530 can create more realistic initial ash cloud and ash parcel positions, and therefore improve the accuracy of
531 ash transport forecasts. Informal sensitivity analyses suggest that initial conditions, as expressed in the
532 disposition of initial ash parcel positions in the vertical, have a more significant effect on a volcanic ash
533 transport forecast than most other parameters. Comparison of initial ash parcel distributions among the
534 3D plume model, semiempirical expressions, and observations suggests that a major subpopulation of ash
535 parcels should be placed at a much lower elevation than plume height to obtain a better VATD forecast.
536 Comparing the effects of the plume height, vertical spread and horizontal spread shows that ash particle
537 distribution in the vertical direction has the strongest effect on VATD simulation results.

538 To summarize, we have presented a novel method for creating *a priori* initial source conditions for
539 VATD simulations. We have shown that it might be possible to obtain initial positions of ash parcels
540 with deterministic forward modeling of the volcanic plume, potentially obviating or lessening the need to
541 attempt to somehow observe initial positions, or *a posteriori* create a history of release heights via inversion
542 (Stohl et al., 2011). Although the method now suffers from the high computational cost associated with
543 3D forward modeling, there is the possibility that in future it might not only help overcome shortcomings
544 of existing methods used to generate *a priori* input parameters, but also overcome the need to carry out
545 thousands of runs associated with inverse modeling. In addition, computational cost will continue to
546 diminish as computing speed increases. As they are forward numerical models based on first principles,
547 3D plume models need little if any parameterization, and user intervention should not be required to
548 improve forecast power; no assumption about the initial position of ash parcels is needed. Generation of the
549 initial cloud of ash parcels directly by 3D simulation is potentially adaptable to a variety of volcanic and
550 atmospheric scenarios. In contrast, semiempirical expressions used to determine initial conditions require
551 several parameters to control ash particle distribution along a vertical line source or some simplified shape

552 of the initial ash cloud, making it difficult in some cases to generate initial conditions that closely resemble
553 a complex reality.

554 The plume-VATD coupling presented in this paper is Lagrangian-Lagrangian coupling. When coupling
555 plume models and VATD models of different types, the interpolation will be different. For example, to
556 couple a Lagarian plume model with an Eulerian VATD model, we must convert the particle distribution in
557 the output of the plume model into ash concentration of cells (mesh grids). When coupling an Eulerian
558 plume model to a Lagrangian VATD model, the mass fraction of the erupted material in the output of the
559 3D plume model should be converted into an ash cloud represented by a group of particles. The steps for
560 coupling a 3D plume model with a VATD model also depends on features of the software, such as the
561 inputs, the outputs, and file formats.

CONFLICT OF INTEREST STATEMENT

562 The authors declare that the research was conducted in the absence of any commercial or financial
563 relationships that could be construed as a potential conflict of interest.

AUTHOR CONTRIBUTIONS

564 The idea of using a 3D plume model to start a VATD simulation originated from a conservation between
565 AP and MB. ZC carried out the Plume-SPH simulations, Puff simulations, initial results analysis, and
566 prepared the first draft. All authors worked together for further revisions. MB carried out the HYSPLIT
567 simulation. QY post-processed the Puff simulation results, overlapped the simulation results with satellite
568 observation, and calculated the FMS values. All authors contributed equally to the manuscript writing. AP
569 and MB obtained funding to financially support the work.

FUNDING

570 This work was supported by National Science Foundation awards 1521855, 1621853, and 1821311,
571 1821338 and 2004302 and by the National Research Foundation Singapore and the Singapore Ministry
572 of Education under the Research Centres of Excellence initiative (project number: NRF2018NRF-
573 NSFC003ES-010).

ACKNOWLEDGMENTS

574 We are grateful to the two anonymous reviewers of the paper for their constructive comments and suggesti-
575 ons that improved the paper. Support for the Twentieth Century Reanalysis Project dataset is provided by
576 the U.S. Department of Energy, Office of Science Innovative and Novel Computational Impact on Theory
577 and Experiment (DOE INCITE) program, and Office of Biological and Environmental Research (BER),
578 and by the National Oceanic and Atmospheric Administration Climate Program Office.

REFERENCES

- 579 Avdyushin, S., Tulinov, G., Ivanov, M., Kuzmenko, B., Mezhuev, I., Nardi, B., et al. (1993). 1. spatial and
580 temporal evolution of the optical thickness of the pinatubo aerosol cloud in the northern hemisphere
581 from a network of ship-borne and stationary lidars. *Geophysical research letters* 20, 1963–1966
582 Beckett, F., Witham, C., Hort, M., Stevenson, J., Bonadonna, C., and Millington, S. (2015). Sensitivity of
583 dispersion model forecasts of volcanic ash clouds to the physical characteristics of the particles. *Journal*
584 *of Geophysical Research: Atmospheres* 120, 11–636
585 Bursik, M. (2001). Effect of wind on the rise height of volcanic plumes. *Geophys. Res. Lett* 28, 3621–3624

- 586 Bursik, M., Jones, M., Carn, S., Dean, K., Patra, A., Pavolonis, M., et al. (2012). Estimation and
587 propagation of volcanic source parameter uncertainty in an ash transport and dispersal model: application
588 to the eyjafjallajokull plume of 14–16 april 2010. *Bulletin of volcanology* 74, 2321–2338
- 589 Bursik, M., Kobs, S., Burns, A., Braitseva, O., Bazanova, L., Melekestsev, I., et al. (2009). Volcanic
590 plumes and wind: Jetstream interaction examples and implications for air traffic. *Journal of Volcanology*
591 and *Geothermal Research* 186, 60–67
- 592 Cao, Z., Patra, A., Bursik, M., Pitman, E. B., and Jones, M. (2018). Plume-sph 1.0: a three-dimensional,
593 dusty-gas volcanic plume model based on smoothed particle hydrodynamics. *Geoscientific Model
594 Development* 11, 2691–2715
- 595 Cao, Z., Patra, A., and Jones, M. (2017). Data management and volcano plume simulation with parallel
596 sph method and dynamic halo domains. *Procedia Computer Science* 108, 786–795
- 597 Cerminara, M., Esposti Ongaro, T., and Berselli, L. (2016a). Ashee-1.0: a compressible, equilibrium-
598 eulerian model for volcanic ash plumes. *Geoscientific Model Development* 9, 697–730
- 599 Cerminara, M., Esposti Ongaro, T., and Neri, A. (2016b). Large eddy simulation of gas–particle kinematic
600 decoupling and turbulent entrainment in volcanic plumes. *Journal of Volcanology and Geothermal
601 Research*
- 602 Constantinescu, R., Hopulele-Gligor, A., Connor, C. B., Bonadonna, C., Connor, L. J., Lindsay, J. M.,
603 et al. (2021). The radius of the umbrella cloud helps characterize large explosive volcanic eruptions.
604 *Communications Earth & Environment* 2, 1–8
- 605 Costa, A., Folch, A., and Macedonio, G. (2013). Density-driven transport in the umbrella region of volcanic
606 clouds: Implications for tephra dispersion models. *Geophysical Research Letters* 40, 4823–4827
- 607 Costa, A., Suzuki, Y., Cerminara, M., Devenish, B., Esposti Ongaro, T., Herzog, M., et al. (2016). Results
608 of the eruptive column model inter-comparison study. *Journal of Volcanology and Geothermal Research*
- 609 D'amours, R. (1998). Modeling the etex plume dispersion with the canadian emergency response model.
610 *Atmospheric Environment* 32, 4335–4341
- 611 Daniele, P., Lirer, L., Petrosino, P., Spinelli, N., and Peterson, R. (2009). Applications of the puff model to
612 forecasts of volcanic clouds dispersal from etna and vesuvio. *Computers & Geosciences* 35, 1035–1049
- 613 DeFoor, T. E., Robinson, E., and Ryan, S. (1992). Early lidar observations of the june 1991 pinatubo
614 eruption plume at mauna loa observatory, hawaii. *Geophysical research letters* 19, 187–190
- 615 de'Michieli Vitturi, M., Neri, A., and Barsotti, S. (2015). Plume-mom 1.0: A new integral model of
616 volcanic plumes based on the method of moments. *Geoscientific Model Development* 8, 2447–2463
- 617 Deshler, T., Hofmann, D., Johnson, B., and Rozier, W. (1992). Balloonborne measurements of the pinatubo
618 aerosol size distribution and volatility at laramie, wyoming during the summer of 1991. *Geophysical
619 research letters* 19, 199–202
- 620 Draxler, R. R. and Hess, G. (1998). An overview of the hysplit.4 modelling system for trajectories.
621 *Australian meteorological magazine* 47, 295–308
- 622 Fero, J., Carey, S. N., and Merrill, J. T. (2008). Simulation of the 1980 eruption of mount st. helens using
623 the ash-tracking model puff. *Journal of Volcanology and Geothermal Research* 175, 355–366
- 624 Fero, J., Carey, S. N., and Merrill, J. T. (2009). Simulating the dispersal of tephra from the 1991
625 pinatubo eruption: implications for the formation of widespread ash layers. *Journal of Volcanology and
626 Geothermal Research* 186, 120–131
- 627 Folch, A., Costa, A., and Macedonio, G. (2009). Fall3d: A computational model for transport and
628 deposition of volcanic ash. *Computers & Geosciences* 35, 1334–1342
- 629 Folch, A., Costa, A., and Macedonio, G. (2016). Fplume-1.0: An integral volcanic plume model accounting
630 for ash aggregation. *Geoscientific Model Development* 9, 431

- 631 Gingold, R. A. and Monaghan, J. J. (1977). Smoothed particle hydrodynamics: theory and application to
632 non-spherical stars. *Monthly notices of the royal astronomical society* 181, 375–389
- 633 Guo, S., Bluth, G. J., Rose, W. I., Watson, I. M., and Prata, A. (2004a). Re-evaluation of so₂ release
634 of the 15 june 1991 pinatubo eruption using ultraviolet and infrared satellite sensors. *Geochemistry,*
635 *Geophysics, Geosystems* 5
- 636 Guo, S., Rose, W. I., Bluth, G. J., and Watson, I. M. (2004b). Particles in the great pinatubo volcanic cloud
637 of june 1991: The role of ice. *Geochemistry, Geophysics, Geosystems* 5
- 638 Holasek, R., Self, S., and Woods, A. (1996a). Satellite observations and interpretation of the 1991 mount
639 pinatubo eruption plumes. *Journal of Geophysical Research: Solid Earth* 101, 27635–27655
- 640 Holasek, R. E., Woods, A. W., and Self, S. (1996b). Experiments on gas-ash separation processes in
641 volcanic umbrella plumes. *Journal of volcanology and geothermal research* 70, 169–181
- 642 Jäger, H. (1992). The pinatubo eruption cloud observed by lidar at garmisch-partenkirchen. *Geophysical*
643 *research letters* 19, 191–194
- 644 Jones, A., Thomson, D., Hort, M., and Devenish, B. (2007). The uk met office's next-generation
645 atmospheric dispersion model, name iii. In *Air pollution modeling and its application XVII* (Springer).
646 580–589
- 647 Mastin, L. G. (2007). A user-friendly one-dimensional model for wet volcanic plumes. *Geochemistry,*
648 *Geophysics, Geosystems* 8
- 649 Mastin, L. G. and Van Eaton, A. R. (2020). Comparing simulations of umbrella-cloud growth and ash
650 transport with observations from pinatubo, kelud, and calbuco volcanoes. *Atmosphere* 11, 1038
- 651 Mastin, L. G., Van Eaton, A. R., and Lowenstern, J. B. (2014). Modeling ash fall distribution from a
652 yellowstone supereruption. *Geochemistry, Geophysics, Geosystems* 15, 3459–3475
- 653 Neri, A., Esposti Ongaro, T., Macedonio, G., and Gidaspow, D. (2003). Multiparticle simulation of
654 collapsing volcanic columns and pyroclastic flow. *Journal of Geophysical Research: Solid Earth*
655 (1978–2012) 108
- 656 Oberhuber, J. M., Herzog, M., Graf, H.-F., and Schwanke, K. (1998). Volcanic plume simulation on large
657 scales. *Journal of Volcanology and Geothermal Research* 87, 29–53
- 658 Osman, S., Beckett, F., Rust, A., and Snee, E. (2020). Sensitivity of volcanic ash dispersion modelling to
659 input grain size distribution based on hydromagmatic and magmatic deposits. *Atmosphere* 11, 567
- 660 Paladio-Melosantos, M. L. O., Solidum, R. U., Scott, W. E., Quiambao, R. B., Umbal, J. V., Rodolfo, K. S.,
661 et al. (1996). Tephra falls of the 1991 eruptions of mount pinatubo. *Fire and mud* 12000, 12030
- 662 Pfeiffer, T., Costa, A., and Macedonio, G. (2005). A model for the numerical simulation of tephra fall
663 deposits. *Journal of Volcanology and Geothermal Research* 140, 273–294
- 664 Pouget, S., Bursik, M., Johnson, C. G., Hogg, A. J., Phillips, J. C., and Sparks, R. S. J. (2016a).
665 Interpretation of umbrella cloud growth and morphology: implications for flow regimes of short-lived
666 and long-lived eruptions. *Bulletin of Volcanology* 78, 1–19
- 667 Pouget, S., Bursik, M., Singla, P., and Singh, T. (2016b). Sensitivity analysis of a one-dimensional model
668 of a volcanic plume with particle fallout and collapse behavior. *Journal of Volcanology and Geothermal*
669 *Research*
- 670 Rolph, G., Stein, A., and Stunder, B. (2017). Real-time environmental applications and display system:
671 Ready. *Environmental Modelling & Software* 95, 210–228
- 672 Schwaiger, H. F., Denlinger, R. P., and Mastin, L. G. (2012). Ash3d: A finite-volume, conservative
673 numerical model for ash transport and tephra deposition. *Journal of Geophysical Research: Solid Earth*
674 117

- 675 Scollo, S., Folch, A., and Costa, A. (2008). A parametric and comparative study of different tephra fallout
676 models. *Journal of Volcanology and Geothermal Research* 176, 199–211
- 677 Scott, W. E., Hoblitt, R. P., Torres, R. C., Self, S., Martinez, M. M. L., and Nillos, T. (1996). Pyroclastic
678 flows of the june 15, 1991, climactic eruption of mount pinatubo. *Fire and Mud: eruptions and lahars of
679 Mount Pinatubo, Philippines*, 545–570
- 680 Searcy, C., Dean, K., and Stringer, W. (1998). Puff: A volcanic ash tracking and prediction model. *Journal
681 of Volcanology and Geothermal Research* 80, 1–16
- 682 Self, S., Zhao, J.-X., Holasek, R. E., Torres, R. C., and King, A. J. (1996). The atmospheric impact of the
683 1991 mount pinatubo eruption
- 684 Stefanescu, E., Patra, A. K., Bursik, M., Jones, M., Madankan, R., Pitman, E. B., et al. (2014). Fast
685 construction of surrogates for uq central to dddas—application to volcanic ash transport. *Procedia
686 Computer Science* 29, 1227–1235
- 687 Stein, A., Draxler, R., Rolph, G., Stunder, B., Cohen, M., and Ngan, F. (2015). Noaa's hysplit atmospheric
688 transport and dispersion modeling system. *Bulletin of the American Meteorological Society* 96, 2059–
689 2077
- 690 Stohl, A., Prata, A., Eckhardt, S., Clarisse, L., Durant, A., Henne, S., et al. (2011). Determination of
691 time-and height-resolved volcanic ash emissions and their use for quantitative ash dispersion modeling:
692 the 2010 eyjafjallajökull eruption. *Atmospheric Chemistry and Physics* 11, 4333–4351
- 693 Suzuki, T. et al. (1983). A theoretical model for dispersion of tephra. *Arc volcanism: physics and tectonics*
694 95, 113
- 695 Suzuki, Y. and Koyaguchi, T. (2009). A three-dimensional numerical simulation of spreading umbrella
696 clouds. *Journal of Geophysical Research: Solid Earth (1978–2012)* 114
- 697 Suzuki, Y. J., Koyaguchi, T., Ogawa, M., and Hachisu, I. (2005). A numerical study of turbulent mixing
698 in eruption clouds using a three-dimensional fluid dynamics model. *Journal of Geophysical Research:
699 Solid Earth* 110
- 700 Tanaka, H. (1991). Development of a prediction scheme for the volcanic ash fall from redoubt volcano. In
701 *First Int'l. Symp. on Volcanic Ash and Aviation Safety*. vol. 58
- 702 Tupper, A., Itikarai, I., Richards, M., Prata, F., Carn, S., and Rosenfeld, D. (2007). Facing the challenges of
703 the international airways volcano watch: the 2004/05 eruptions of manam, papua new guinea. *Weather
704 and Forecasting* 22, 175–191
- 705 Walko, R., Tremback, C., and Bell, M. (1995). Hypact: The hybrid particle and concentration transport
706 model. *User's guide*
- 707 Webster, H. N., Devenish, B. J., Mastin, L. G., Thomson, D. J., and Van Eaton, A. R. (2020). Operational
708 modelling of umbrella cloud growth in a lagrangian volcanic ash transport and dispersion model.
709 *Atmosphere* 11, 200
- 710 Witham, C., Hort, M., Potts, R., Servranckx, R., Husson, P., and Bonnardot, F. (2007). Comparison of
711 vaac atmospheric dispersion models using the 1 november 2004 grimsvötn eruption. *Meteorological
712 Applications* 14, 27–38
- 713 Woods, A. (1988). The fluid dynamics and thermodynamics of eruption columns. *Bulletin of Volcanology*
714 50, 169–193
- 715 Zidikheri, M. J., Lucas, C., and Potts, R. J. (2017). Estimation of optimal dispersion model source
716 parameters using satellite detections of volcanic ash. *Journal of Geophysical Research: Atmospheres*
717 122, 8207–8232

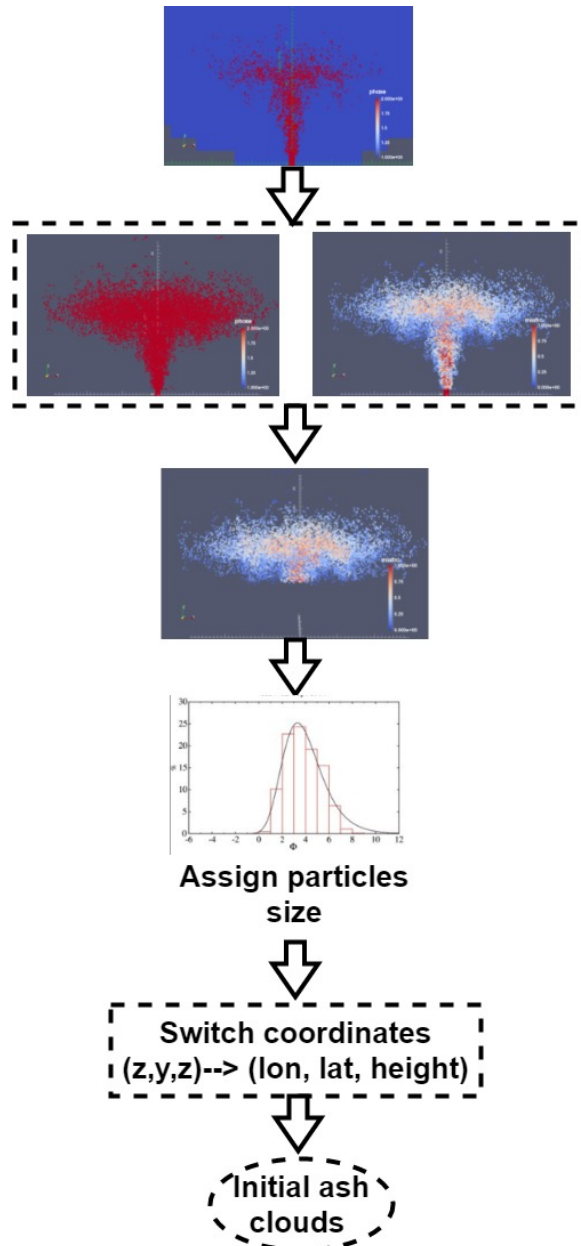


Figure 1. Steps to create initial condition for Puff based on raw output of Plume-SPH (Cao et al., 2018). First row: raw output of Plume-SPH. Blue particles are phase 1 (ambient air), red particles are phase 2 (erupted material). Second row: plume after removing SPH particles of phase 1. Picture at right is colored according to the mass fraction of erupted material. Third row: volcanic plume above the “corner” region after cutting off the lower portion. Fourth row: assign sizes to particles converting numerical discretization points into tracers. Fifth row: switch coordinates in local coordinate system into (*longitude, latitude, height*)

FIGURE CAPTIONS

718 T

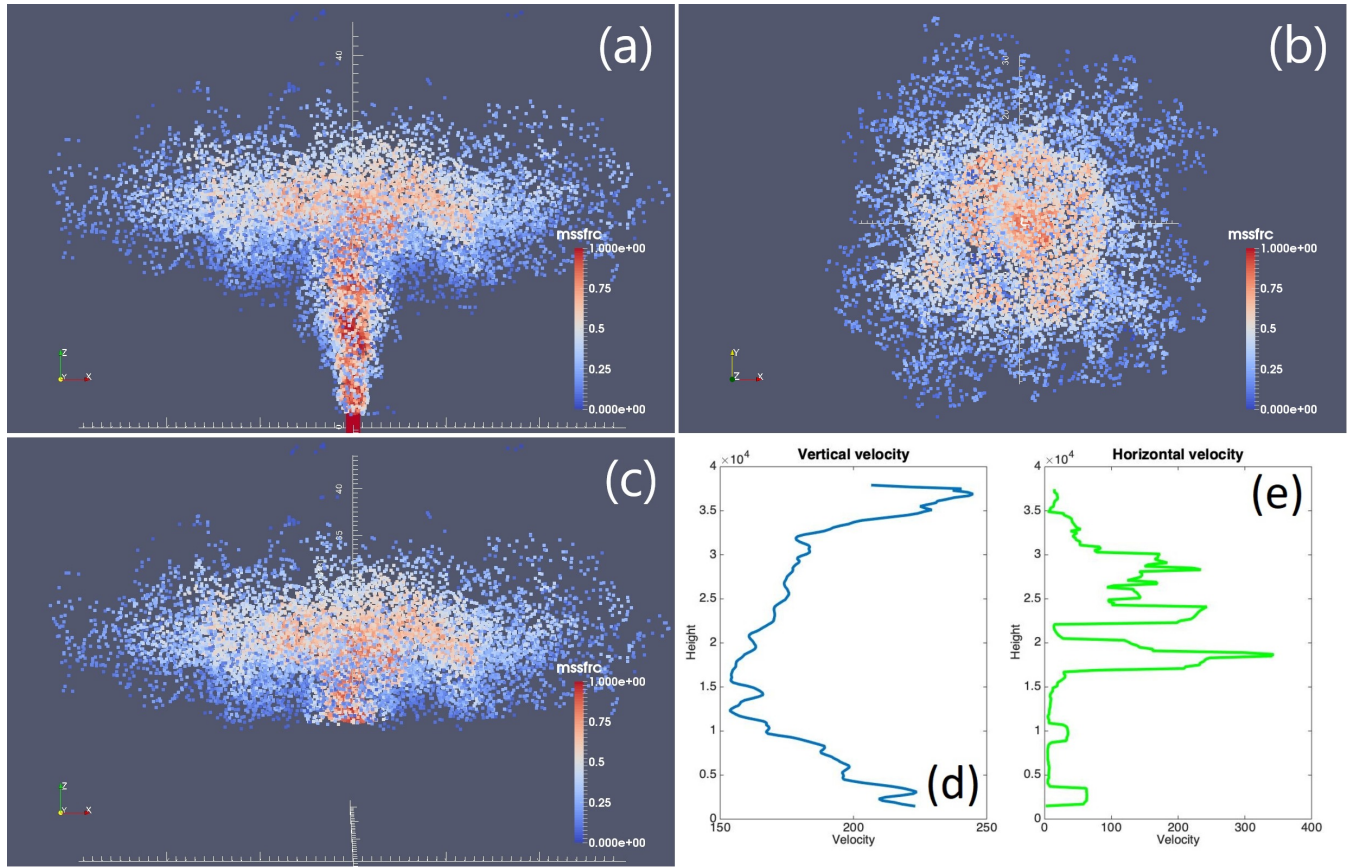


Figure 2. Volcano plume from 3D plume model. All particles in the pictures are of phase 2 (particle of phase 1 has been removed) at 600s after eruption, at which time, the plume has already reached the plume height and started spreading radially. (a) is the front view of the whole plume. (b) is the top view of the plume. (c) is the front view of the initial ash cloud, which is essentially a portion of the whole plume whose elevation is higher than a given threshold (in this picture is 15 km). Particles are colored according to mass fraction of erupted material. Red represents high mass fraction while blue represents low mass fraction. (d) is the average vertical velocity of the plume. At elevations below 15 km, the average vertical velocity decreases. At elevations higher than 15 km, the averaged vertical velocity starts increasing. (e) is the average horizontal velocity of the plume. The averaged horizontal velocity becomes obviously larger when elevation is higher than 15 km. So the reflection point is somewhere around 15 km.

Table 1. List of eruption condition and material properties for plume simulation

Parameters	Units	Plume
Vent Velocity	$\text{m} \cdot \text{s}^{-1}$	275
Vent Gas Mass Fraction		0.05
Vent Temperature	K	1053
Vent Height	m	1500
Mass Discharge Rate	$\text{kg} \cdot \text{s}^{-1}$	1.5×10^9
Specific Heat of Gas at Constant Volume	$\text{J} \cdot \text{kg}^{-1} \cdot \text{K}^{-1}$	717
Specific Heat of Air at Constant Volume	$\text{J} \cdot \text{kg}^{-1} \cdot \text{K}^{-1}$	1340
Specific Heat of Solid	$\text{J} \cdot \text{kg}^{-1} \cdot \text{K}^{-1}$	1100
Specific Heat of Gas at Constant Pressure	$\text{J} \cdot \text{kg}^{-1} \cdot \text{K}^{-1}$	1000
Specific Heat of Air at Constant Pressure	$\text{J} \cdot \text{kg}^{-1} \cdot \text{K}^{-1}$	1810
Density of Air at Vent Height	$\text{kg} \cdot \text{m}^{-3}$	1.104
Pressure at Vent Height	Pa	84363.4

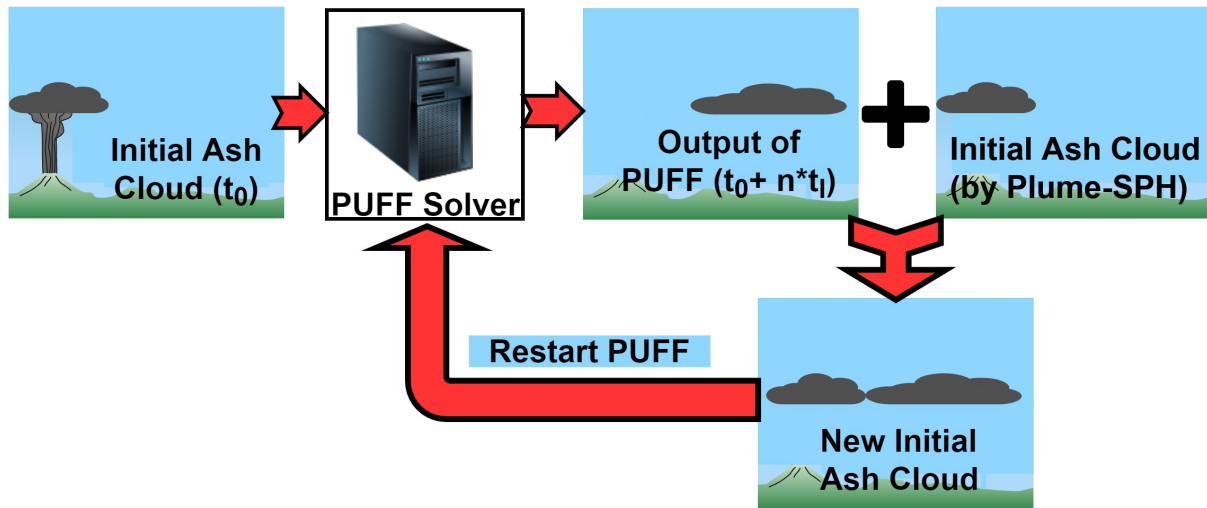


Figure 3. Mimic successive eruption with intermittent pulsed releasing of ash particles. t_I is the period of pulsing release. t_I equals the physical time of 3D plume simulation.

Table 2. Parameters used in VATD simulation of the climactic phase of Pinatubo eruption on June 15 1991. The first six parameters are used by semiempirical expression to create an initial ash cloud. When creating an initial condition based on the Plume-SPH model, these parameters are extracted from output of Plume-SPH model.

Parameters	Unit	Semiempirical	Plume-SPH
Plume Height (H_{max})	km	40	-
Horizontal Spread (r_{max})	km	103.808	-
Vertical Spread (H_{width})	km	6.662	-
Plume Shape	-	Poisson	-
Total Ash Particles	-	1768500	1768500
Elevation Threshold	m	-	15000
Horizontal Diffusivity	m^2/s	10000	10000
Vertical Diffusivity	m^2/s	10	10
Grain Size Distribution	-	Gaussian	Gaussian
Mean of Grain Size (Radius)	mm	3.5×10^{-2}	3.5×10^{-2}
Standard Deviation of Grain Size	-	1.0	1.0
Start Time	UT	0441	0441
End time	UT	1341	1341
Simulation Duration	hour	72	72

Table 3. The starting and ending time (UT) for simulating the climactic phase of Pinatubo eruption on June 15 1991. Observed plume height (Holasek et al., 1996a) at different time are also listed in the table.

Eruption Duration	4.9 hours	9 hours	10 hours	11.1 hours
Start Time	0441	0441	0441	0334
Height at Start Time	37.5 km	37.5 km	37.5 km	24.5 km
End Time	0934	1341	1441	1441
Height at End Time	35 km	26.5 km	22.5	22.5 km

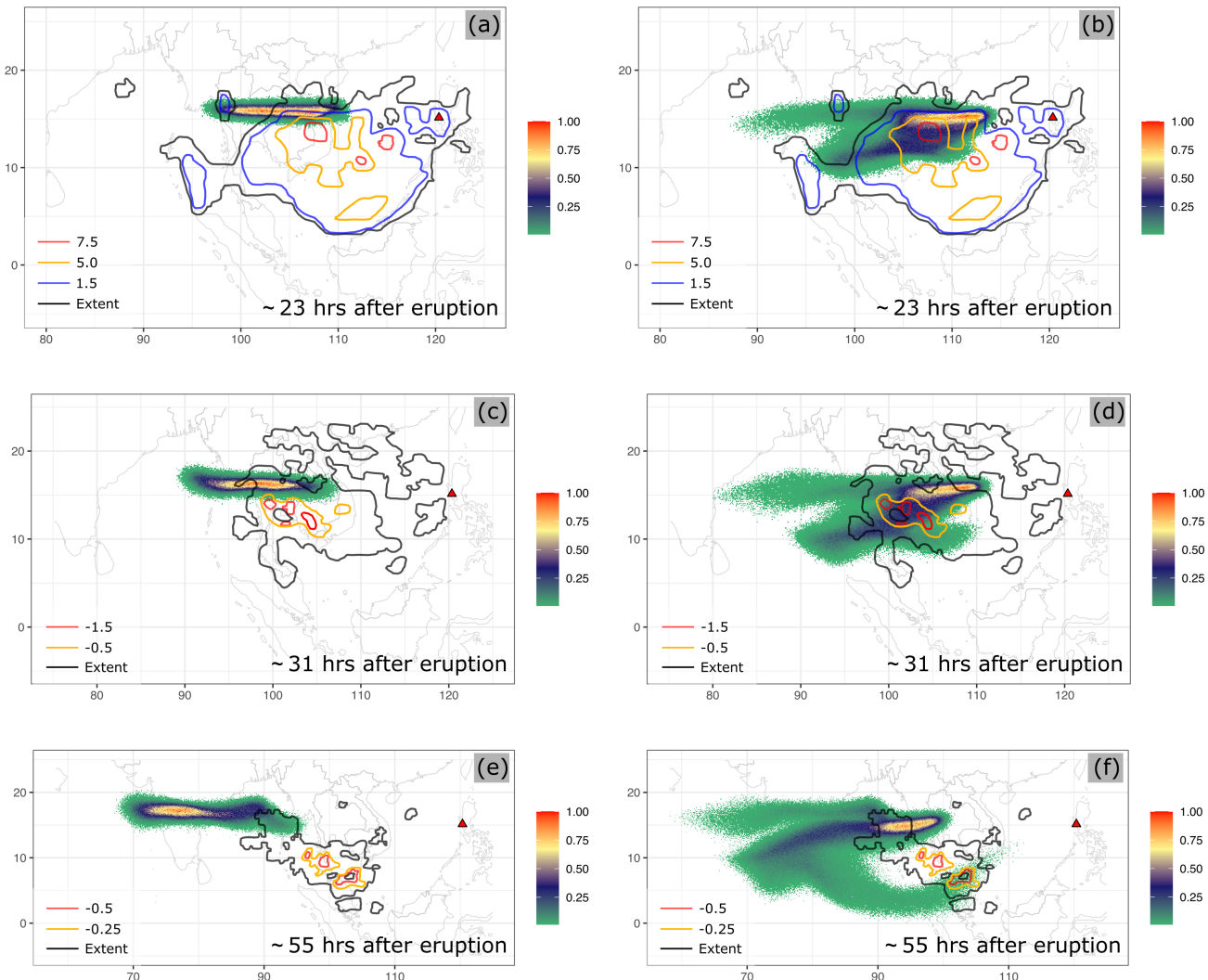


Figure 4. Comparison between “Semiempirical initial cloud + Puff” and “Plume-SPH + Puff”. Pictures to the left are: Puff simulation based on initial condition created according to semiempirical plume shape expression. Pictures to the right are Puff simulation based on initial conditions generated by Plume-SPH. TOMS or AVHRR images of Pinatubo ash cloud are overlapped with the simulation results. Ash clouds at different hours after eruption are on different rows. From top to bottom, the images correspond to around 23 hours after eruption (UT 199106160341), 31 hours after eruption (UT 199106161141), 55 hours after eruption (UT 199106171141). The observation data on the first row are TOMS ash and ice map. The observation data on the second and third row are AVHRR BTD ash cloud map with atmospheric correction method applied (Guo et al., 2004b). The contours of simulation results are maximum concentration at given (*longitude, latitude*).

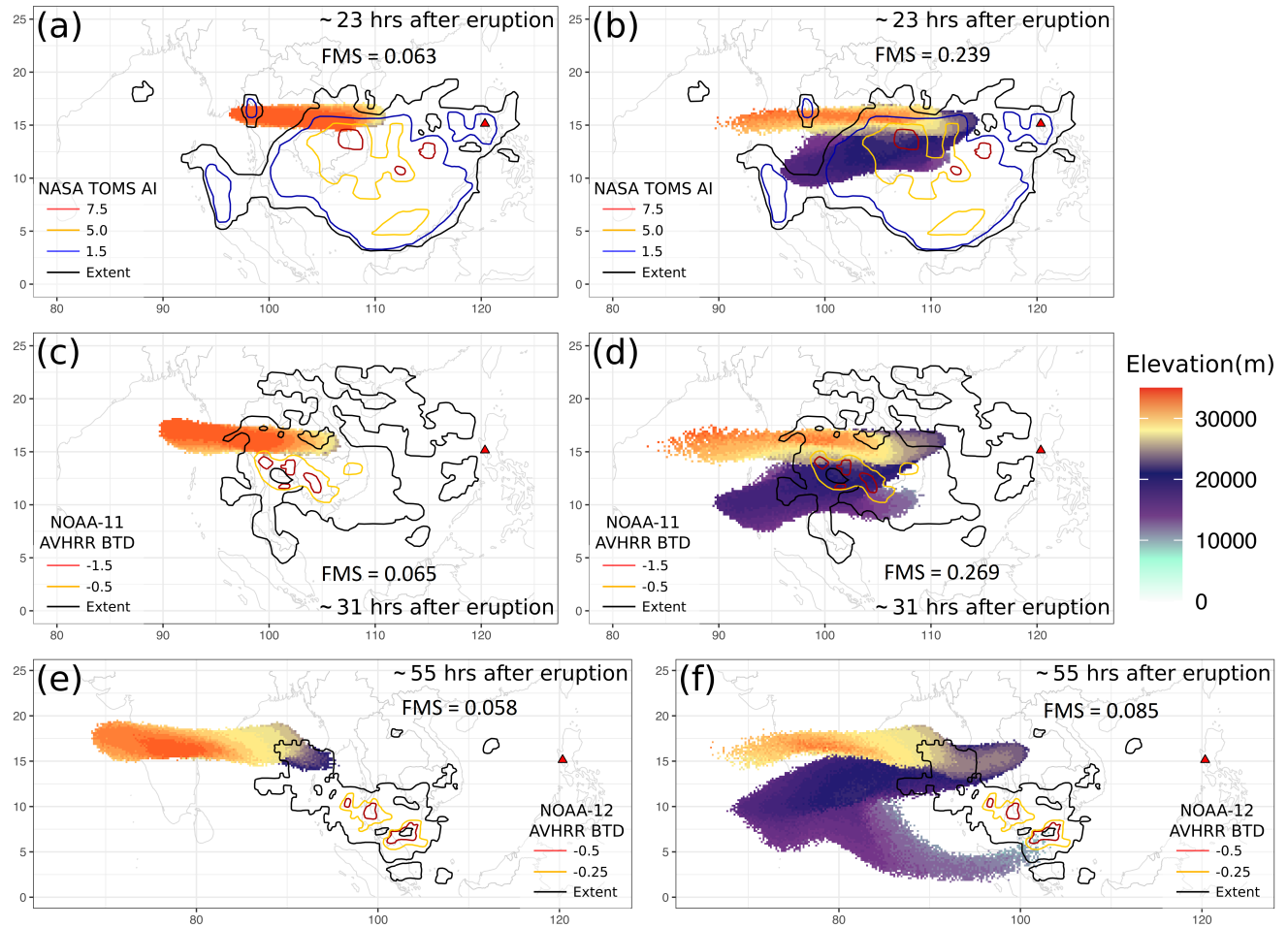


Figure 5. Comparison between “Semiempirical initial cloud + Puff” and “Plume-SPH + Puff”. Pictures to the left are: Puff simulation based on initial condition created according to semiempirical plume shape expression. Pictures to the right are Puff simulation based on initial conditions generated by Plume-SPH. TOMS or AVHRR images of Pinatubo ash cloud are overlapped with the simulation results. Ash clouds at different hours after eruption are on different rows. From top to bottom, the images correspond to around 23 hours after eruption (UT 199106160341), 31 hours after eruption (UT 199106161141), 55 hours after eruption (UT 199106171141). The observation data on the first row are TOMS ash and ice map. The observation data on the second and third row are AVHRR BTD ash cloud map with atmospheric correction method applied (Guo et al., 2004b). The contours of simulation results are maximum height of ash cloud. The FMS value for each simulation is on each contour.

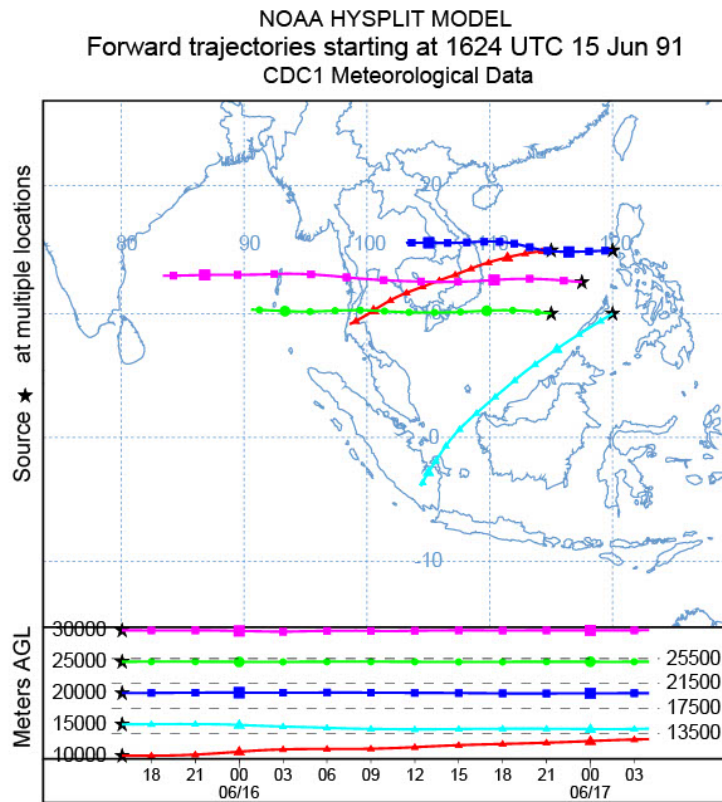


Figure 6. Trajectories of particles starting from different heights indicating the wind directions of different evaluations. The trajectories are chosen to start at points that were on the perimeter of the umbrella cloud in x , y and z , and in its center, right before it became affected by the wind to give an idea of the maximum possible spread of the trajectories from that initial condition.

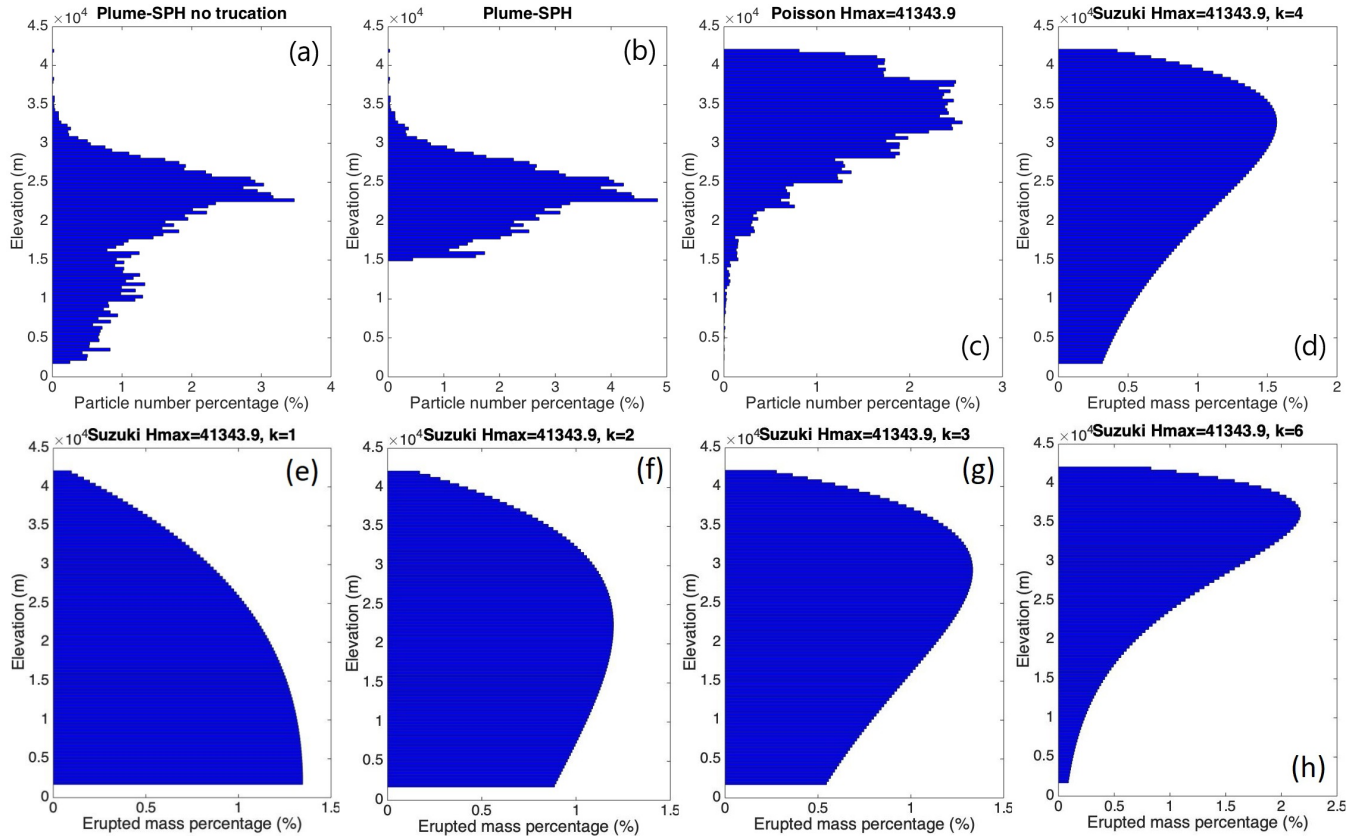


Figure 7. First row, comparison of particle distribution of initial ash cloud in vertical direction. (a) is corresponding to the initial ash cloud obtained from Plume-SPH output. (b) is (a) truncated by a elevation threshold of 15 km. (c) is for vertical ash distribution based on Poisson distribution (Eq. (13)) with H_{max} equals to 40 km. Another parameter, H_{width} is 6662 m. (d) is corresponding to Suzuki distribution (Eq. (14)) with H_{max} equals to 40 km and k equals to 4(Pfeiffer et al., 2005). The second row, Suzuki distribution with H_{max} equals to 40 km but different values for k . The x axis is the percentage of particle numbers for Plume-SPH and Poisson. For Suzuki the x axis is the mass percentage of erupted material.

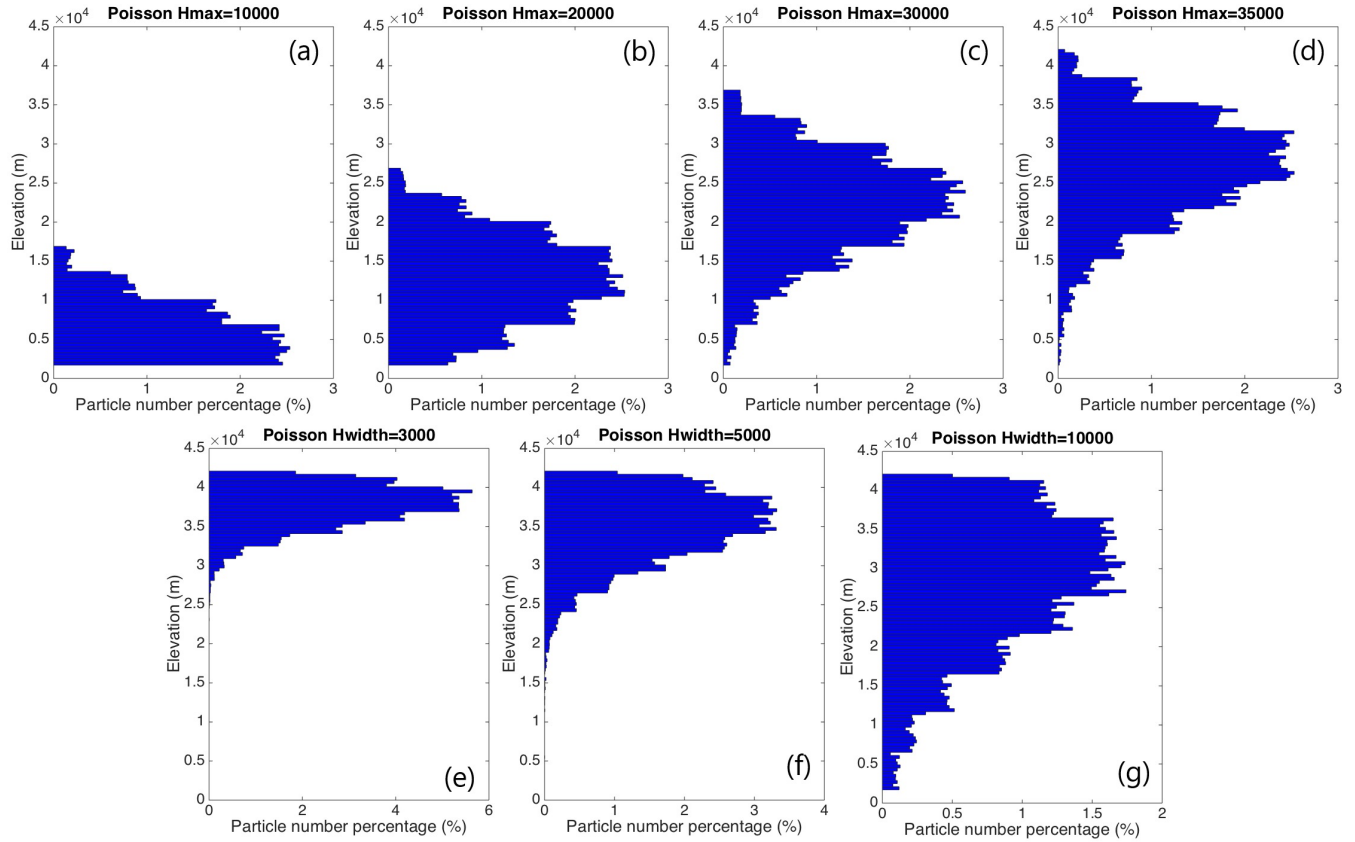


Figure 8. Initial particle distribution in vertical direction based on Poisson plume shape (Eq. (13)). The first row varies plume heights. (a) to (d) are corresponding to plume height of 10 km, 20 km, 30 km, 35 km. Another parameter, H_{width} is 6662 m for all four figures in the first row. The second row varies “vertical spread”, H_{width} . (e) to (g) are corresponding to vertical spread of 3 km, 5 km and 10 km. The plume height, H_{max} is set to 40 km for all three figures. The x axis is the percentage of particle numbers. See Fig. 7 for vertical ash distribution of Plume-SPH output.

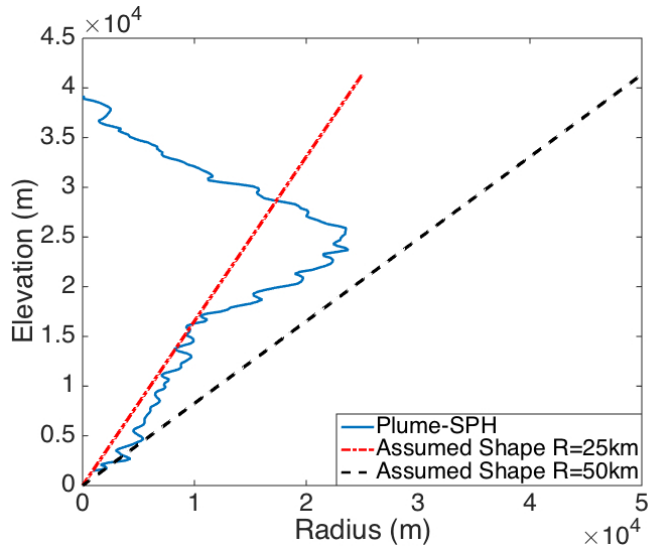


Figure 9. Comparison between radius of initial ash clouds created by 3D plume model (Plume-SPH) and assumed initial ash cloud shape (Eq. 15) in Puff. The plume shape expression used in Puff defines an inverted cone whose actual shape changes when “horizontal spread” takes different values. $R = 25$ km is corresponding to “horizontal spread” equals to 50 km. $R = 50$ km is corresponding to “horizontal spread” equals to 100 km

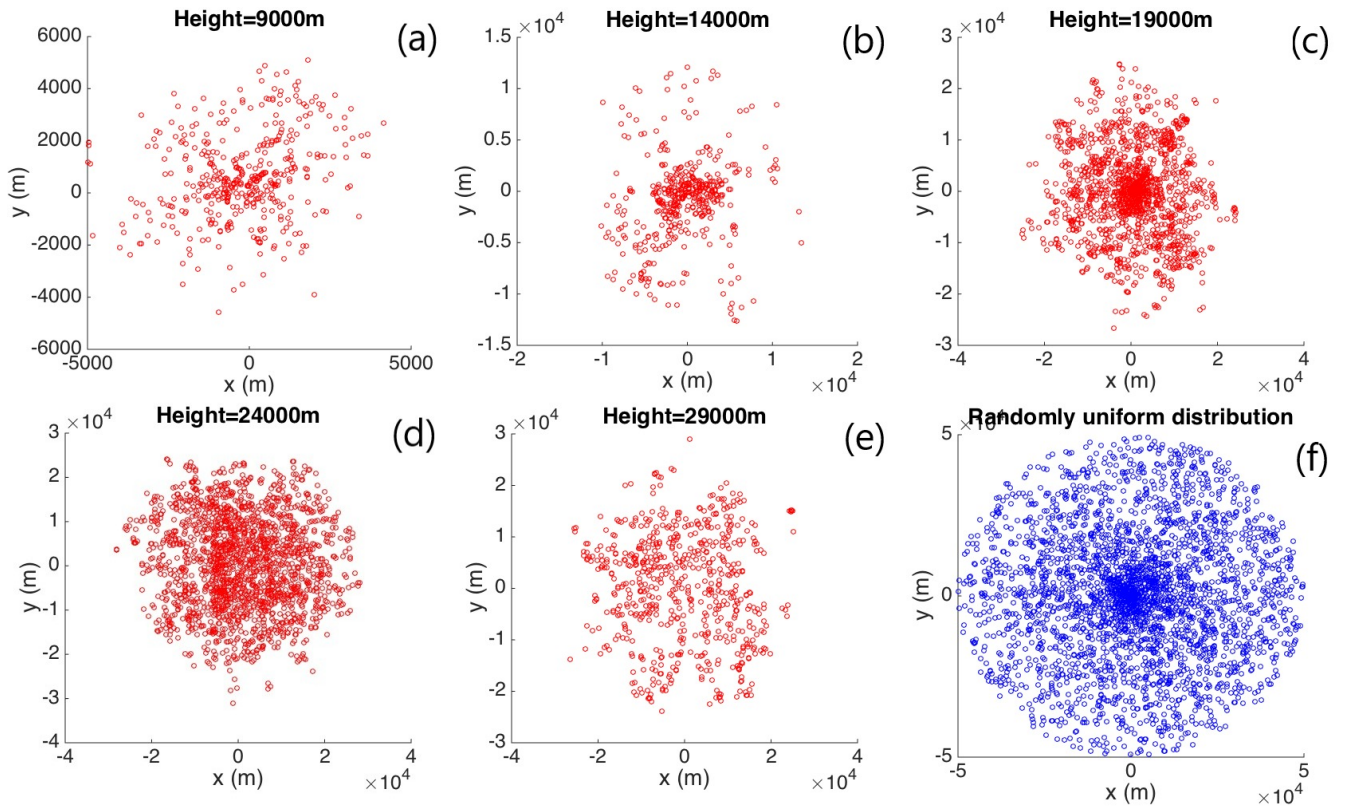


Figure 10. Horizontal distribution of ash particles (tracers) on a cross section of initial ash cloud. Puff assumes a randomly uniform distribution of ash particles within a circle, as shown by blue dots in (f). All other figures show the ash particle distribution of initial ash clouds created by Plume-SPH at different elevations.

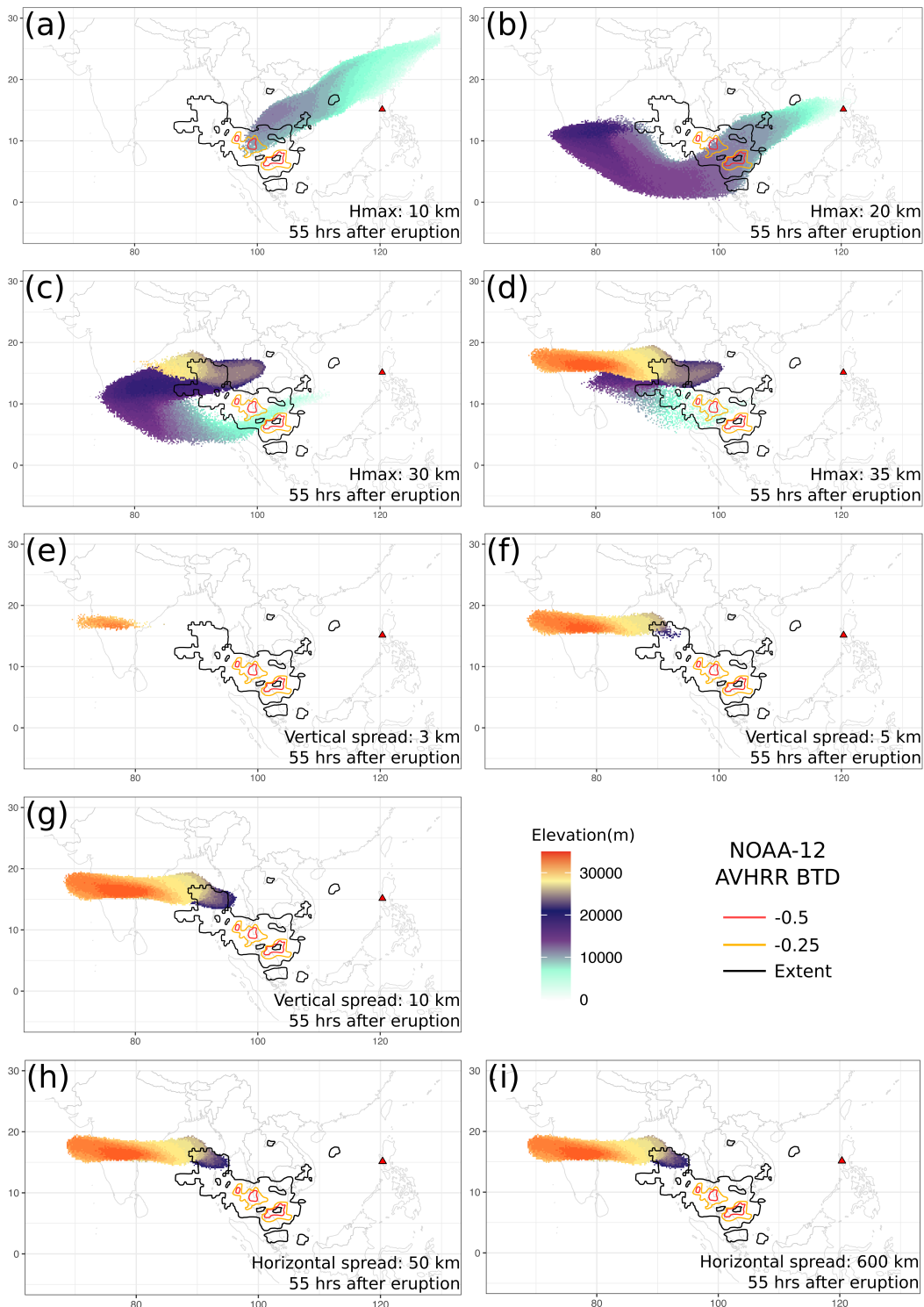


Figure 11. Ash transport simulated by Puff using different initial ash clouds created according the empirical expressions using different input parameters. All images are corresponding to 55 hours after eruption (UT 199106171141). More details are in the table below

Parameter	H_{max}				H_{width}			r_{max}	
	10 km	20 km	30 km	35 km	3 km	5 km	10 km	50 km	600 km
Value	0.055	0.121	0.142	0.227	0	0.039	0.085	0.073	0.074
Plot	(a)	(b)	(c)	(d)	(e)	(f)	(g)	(h)	(i)
FMS									

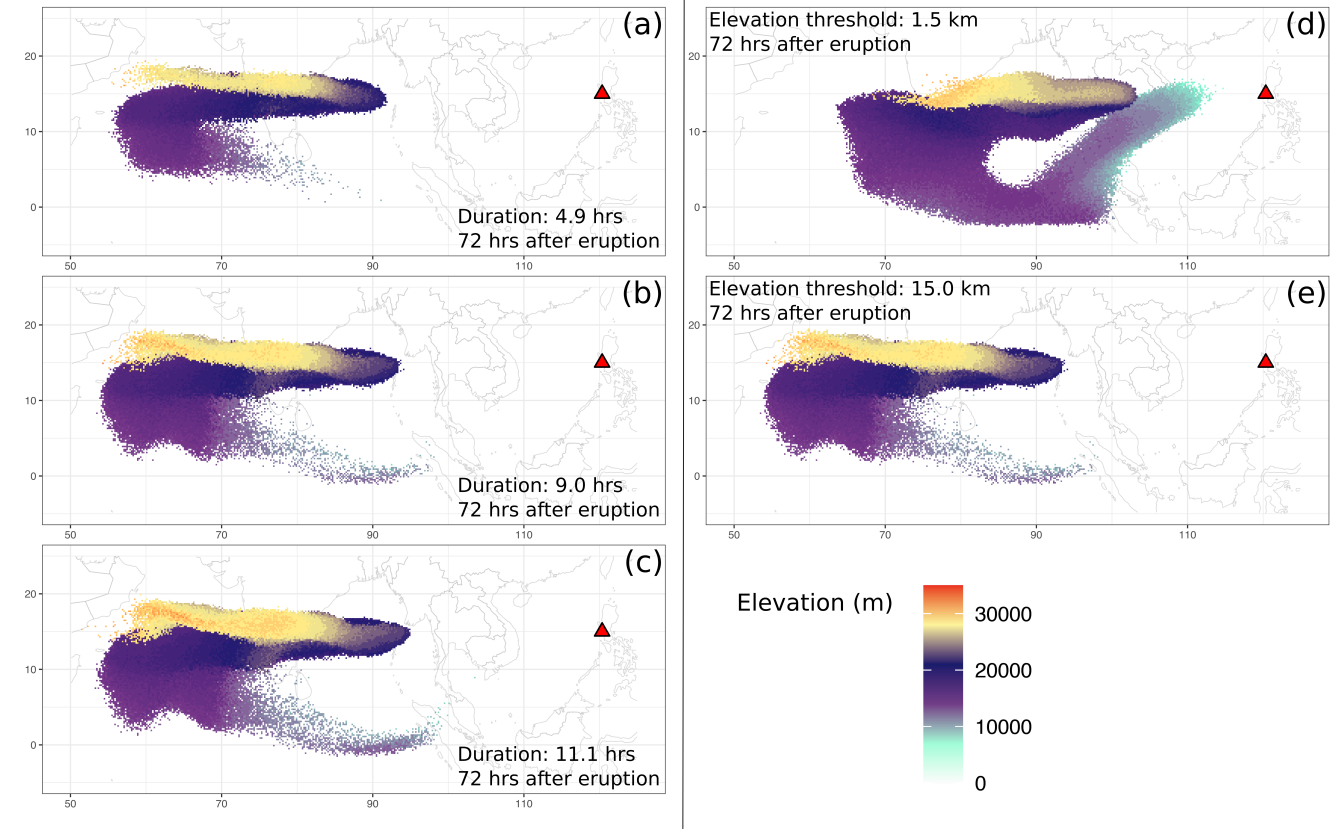


Figure 12. Sensitivity of Puff simulation with respect to eruption durations and initial ash cloud cutoff heights (elevation threshold). For different eruption durations, the starting and ending time for each case is in Table 3. The contours correspond to ash concentration at 72 hours after eruption. Details are in the table below.

Parameter	Eruption Duration			Elevation Threshold	
Value	4.9 hour	9 hour	11.1 hour	1500 m	15 km
Plot	(a)	(b)	(c)	(d)	(e)